© 2021. Published by The Company of Biologists Ltd | Journal of Cell Science (2021) 134, jcs258465. doi:10.1242/jcs.258465

RESEARCH ARTICLE

Distinct temporal expression of the GW182 paralog TNRC6A in neurons regulates dendritic arborization

Bharti Nawalpuri[1,2,3], Arpita Sharma[1], Sumantra Chattarji[4,5] and Ravi S. Muddashetty[1,3,*]

ABSTRACT

Precise development of the dendritic architecture is a critical determinant of mature neuronal circuitry. MicroRNA (miRNA)-mediated regulation of protein synthesis plays a crucial role in dendritic morphogenesis, but the role of miRNA-induced silencing complex (miRISC) protein components in this process is less studied. Here, we show an important role of a key miRISC protein, the GW182 paralog TNRC6A, in the regulation of dendritic growth. We identified a distinct brain region-specific spatiotemporal expression pattern of GW182 during rat postnatal development. We found that the window of peak GW182 expression coincides with the period of extensive dendritic growth, both in the hippocampus and cerebellum. Perturbation of GW182 function during a specific temporal window resulted in reduced dendritic growth of cultured hippocampal neurons. Mechanistically, we show that GW182 modulates dendritic growth by regulating global somatodendritic translation and actin cytoskeletal dynamics of developing neurons. Furthermore, we found that GW182 affects dendritic architecture by regulating the expression of actin modulator LIMK1. Taken together, our data reveal a previously undescribed neurodevelopmental expression pattern of GW182 and its role in dendritic morphogenesis, which involves both translational control and actin cytoskeletal rearrangement.

This article has an associated First Person interview with the first author of the paper.

KEY WORDS: Cytoskeleton, Dendritic development, GW182, TNRC6A, LIMK1, Neurons, Translation regulation

INTRODUCTION

Dendrites are the primary sites of information reception and integration in neurons. Precise development of the dendritic architecture is crucial for the establishment of neuronal circuitry. Consequently, defects in dendritic arborization are a common feature of multiple neurodevelopmental disorders (Kulkarni and Firestein, 2012; Martínez-Cerdeño, 2017).

The development of dendritic arborization is a multistep process with overlapping events of polarity establishment, dendritic extension, dendritic branching and pruning, as well as stabilization (Arikkath, 2012). These events are controlled by intrinsic factors as well as extracellular cues via transcriptional and post-transcriptional gene regulatory mechanisms (Dong et al., 2015; Jan and Jan, 2010). Among these, translation regulation is one of the key mechanisms employed by neurons to control dendritic development (Chihara et al., 2007; Jaworski et al., 2005; Kumar et al., 2005; Lein and Higgins, 1991; Ravindran et al., 2019; Slomnicki et al., 2016; Xing et al., 2012). Often, these translation regulatory pathways converge on modulation of cytoskeletal dynamics for the regulation of dendritic arborization (Perycz et al., 2011; Ravindran et al., 2019).

Evidence highlighting the importance of translation regulation in dendritic development primarily comes from studies involving RNA-binding proteins (RBPs). Multiple RBPs that regulate translation, such as ZBP1, Pumilio, Nanos, CPEB1, FMRP (also known as FMR1), MOV10 and Staufen have been implicated in the regulation of dendritic development (Bestman and Cline, 2008; Brechbiel and Gavis, 2008; Lee et al., 2003; Perycz et al., 2011; Ye et al., 2004). Notably, many of these RBPs modulate the translation of cytoskeletal regulators for controlling dendritic morphogenesis. Interestingly, many of these RBPs, such as FMRP, Pumilio, MOV10, and CPEB1, act as ancillary components of the microRNA-induced silencing complex (miRISC) to regulate miRNA-mediated gene silencing (Banerjee et al., 2009; Ford et al., 2019; Kenny et al., 2014; Nawalpuri et al., 2020; Sternburg et al., 2018).

MicroRNAs (miRNAs) are 21–23-nucleotide-long non-coding RNA molecules involved in post-transcriptional regulation of gene expression (Bartel, 2018; Gebert and MacRae, 2019; Kosik, 2006; McNeill and Van Vactor, 2012; Rajman and Schratt, 2017; Ramakrishna and Muddashetty, 2019). The regulatory functions of microRNAs are executed by associating with the multi-protein miRISC complex. GW182 proteins (TNRC6A, TNRC6B and TNRC6C in mammals) and AGO2 are core miRISC proteins that work in conjunction with the ancillary components such as the CCR4–NOT complex, decapping complex, XRN1, MOV10, and FMRP (Bartel, 2018; Duchaine and Fabian, 2019; Filipowicz et al., 2008). These protein components associate to form functionally diverse miRISC complexes (Nawalpuri et al., 2020). The protein composition of miRISC is an important determinant of its kinetics and reversibility, thereby determining the ability of miRISC to respond to external cues. Such cue-dependent modulation of miRISC composition is crucial in regulating synaptic plasticity. However, the significance of miRISC composition has not been studied in the context of neurodevelopment. Importantly, due to its scaffolding function, GW182 plays a crucial role in determining the composition of the miRISC.

GW182, an evolutionarily conserved scaffolding protein, is a key component of metazoan miRISC (Ding and Han, 2007; Niaz and Hussain, 2018; Zielezinski and Karlowski, 2015). It is involved in the recruitment of deadenylation, decapping and degradation enzymes to the AGO2–miRNA–mRNA complex (Eulalio et al., 2009).

[1]Centre for Brain Development and Repair, Institute for Stem Cell Science and Regenerative Medicine (InStem), Bangalore 560065, India. [2]School of Chemical and Biotechnology, Shanmugha Arts, Science, and Technology and Research Academy (SASTRA) University, Thanjavur 613401, India. [3]Centre for Brain Research, Indian Institute of Science, Bangalore 560012, India. [4]National Centre for Biological Sciences, Bangalore 560065, India. [5]Simons Initiative for the Developing Brain and Centre for Discovery Brain Sciences, University of Edinburgh EH8 9XD, Edinburgh, UK.

*Author for correspondence (ravism@instem.res.in; ravimshetty@iisc.ac.in)

B.N., 0000-0002-9218-0234; R.S.M., 0000-0002-1373-6194

Handling Editor: Giampietro Schiavo
Received 28 January 2021; Accepted 19 July 2021

Journal of Cell Science (2021) 134, jcs258465. doi:10.1242/jcs.258465

Structurally, it contains an N-terminal AGO-binding domain and a C-terminal silencing domain involved in the recruitment of mRNA degradation machinery (Eulalio et al., 2009, 2008; Pfaff et al., 2013). The C-terminal domain of GW182 also binds to the poly(A)-binding protein (PABP) complex, preventing the circularization of mRNA. Despite recent advances in the establishment of GW182 as a central miRISC component, the fundamental role of GW182 in neuronal development and function remains obscure. Here, we show a distinct spatiotemporal expression pattern of the GW182 paralog TNRC6A in the brain. We also describe a novel function of this GW182 paralog in the regulation of dendritic arborization of hippocampal neurons.

RESULTS

GW182 expression follows a distinct spatiotemporal profile during neuronal development

We investigated the expression pattern of miRISC components AGO2, GW182, XRN1, MOV10 and FMRP during rat brain development in two distinct brain regions: hippocampus and cerebellum. In this study, we focused on the GW182 paralog TNR6CA, which we refer to hereafter as GW182. The timeline of different neurodevelopmental processes is well characterized in both these brain regions, providing the opportunity to correlate changes in expression pattern of miRISC proteins to specific neurodevelopmental stages.

Rat hippocampal and cerebellar tissues were harvested at different stages of brain development from embryonic day 18 (E18) to postnatal day 60 (P60) and were subjected to immunoblotting to analyze the expression of miRISC protein components (Fig. 1A). In the hippocampus, the levels of AGO2 significantly increased from E18 to P60 (Fig. 1B), while the expression of MOV10 and XRN1 remained unchanged (Fig. S1B,C). Hippocampal FMRP expression increased 2.5-fold between P5 and P15 and remained unchanged from P15 onwards (Fig. S1A). Interestingly, hippocampal expression of GW182 peaked at P7, followed by a 10-fold reduction in expression from P7 to P15. This reduced expression was sustained from P15 onwards (Fig. 1C).

With cerebellar lysates, similar to the hippocampus, we found that AGO2 expression gradually increased from E18 to P60 (Fig. 1D). Similarly, XRN1 expression also increased significantly from P5 to P30 (Fig. S1F). The cerebellar expression of MOV10 peaked at P7, with a sustained reduction from P15 onward (Fig. S1E). Similar to the hippocampus, FMRP expression also increased 2.8-fold from P5 to P15 in the cerebellum (Fig. S1D). In the cerebellum, GW182 levels peaked at P15, with a gradual reduction in expression level from P15 to P60 (Fig. 1E). Immunoblotting results from cerebellum and hippocampus highlighted one striking feature; in both the regions, the expression of GW182 peaks during the time of extensive dendritic arborization, followed by a significant reduction of expression in the mature tissue. Among all the proteins examined, only GW182 showed this peculiar expression profile.

To understand whether the distinct expression pattern of GW182 is a brain-specific feature, we investigated the expression of GW182 in liver lysates. In the liver, GW182 levels were almost undetectable at P5, with an increase from P5 to P15 (Fig. S1G). The levels remained elevated thereafter. This finding supports the idea of a brain-specific temporal profile of GW182 expression. We also investigated the developmental expression profile of GW182 mRNA, to examine whether it mirrors the protein expression pattern. In the hippocampus, the levels of GW182 mRNA remained unchanged between P7 and P15 (the point of peak GW182 protein expression and period of sustained drop, respectively) (Fig. S1I). In contrast, the AGO2 mRNA expression profile mirrored the protein expression pattern of AGO2 (Fig. S1H). A similar trend was observed in the cerebellum, where GW182 mRNA levels remained unchanged from P15 to P30 (Fig. S1K), whereas AGO2 mRNA levels increased significantly between P5 and P30 (Fig. S1J). This suggests that the expression of GW182 during neuronal development is likely to be regulated at the level of translation.

We further investigated the spatial localization of GW182 during neuronal development. For this, we performed immunohistochemistry in the hippocampal CA1 region at P7 and P15 (the point of peak GW182 protein expression and period of drop in the hippocampus, respectively). The primary cell body layer *stratum pyramidale* was identified using DAPI staining. At P7, GW182 staining was observed in both the *stratum pyramidale* (cell body) and *stratum oriens* (dendritic layer) (Fig. 1F). At P15, we observed reduced GW182 staining in both the layers, with a pronounced reduction in the *stratum oriens* (Fig. 1F). We also examined GW182 expression in cerebellar slices at P15 and P30 (the point of peak GW182 protein expression and period of drop in the cerebellum, respectively). Calbindin was used as a marker to identify Purkinje neuron cell bodies and dendrites. At P15, we observed GW182 expression in all three layers of the cerebellum, namely the granular, Purkinje and molecular layers (Fig. 1G). In contrast, at P30 we observed a drastic reduction in GW182 levels, which was most pronounced in the molecular layer (Fig. 1G). Taken together, these results demonstrate the distinct, brain-specific spatiotemporal expression profile of the miRISC protein GW182.

The spatiotemporal expression pattern of GW182 is recapitulated in hippocampal neuronal culture

In the experiments above, we demonstrated that GW182 follows a distinct spatiotemporal expression profile during brain development. Because GW182 levels peaked during the dendritogenesis period, we wanted to study the role of GW182 in the regulation of dendrite morphology. For this, we selected dissociated hippocampal neuronal cultures as our model system. This system offers several advantages, including accessibility and amenability to molecular and pharmacological manipulations. We first investigated whether the spatiotemporal expression pattern of GW182 is recapitulated in a dissociated culture system. Hippocampal neurons were cultured from embryonic day 18 (E18) rat embryos, as previously described (Kaech and Banker, 2006) (Fig. 2A). Cultured neurons were harvested at different developmental stages [days *in vitro* (DIV) 3, 6, 9, 12, 15 and 21] and subjected to immunoblotting analysis for GW182 protein. GW182 expression could be detected in cultured neurons as early as DIV3. The levels peaked at DIV6, followed by a drastic reduction at DIV9. GW182 levels further reduced significantly from DIV9 to DIV12 (Fig. 2B). The reduced expression of GW182 was maintained in DIV21 mature neurons. Thus, the temporal expression of GW182 in cultured neurons parallels the *in vivo* expression. As a control, we also investigated the developmental expression profile of AGO2 in our culture system. We found that the expression pattern of AGO2 in cultured neurons also mirrored the *in vivo* expression profile (Fig. 2C), with levels of AGO2 significantly increasing from DIV3 to DIV15. Next, we investigated the spatial expression of GW182 in cultured neurons using quantitative immunostaining (Fig. 2D). We measured cytosolic and dendritic levels of GW182 in cultured neurons at DIV6 (point of peak expression) and DIV 12 (period after which GW182 levels do not drop further). We observed a significant reduction in cytosolic as well as dendritic levels of GW182 from DIV6 to DIV12 (Fig. 2D–F). Hereby, we conclude that the spatiotemporal expression pattern of GW182 is recapitulated in dissociated hippocampal neuronal cultures.

Journal of Cell Science (2021) 134, jcs258465. doi:10.1242/jcs.258465

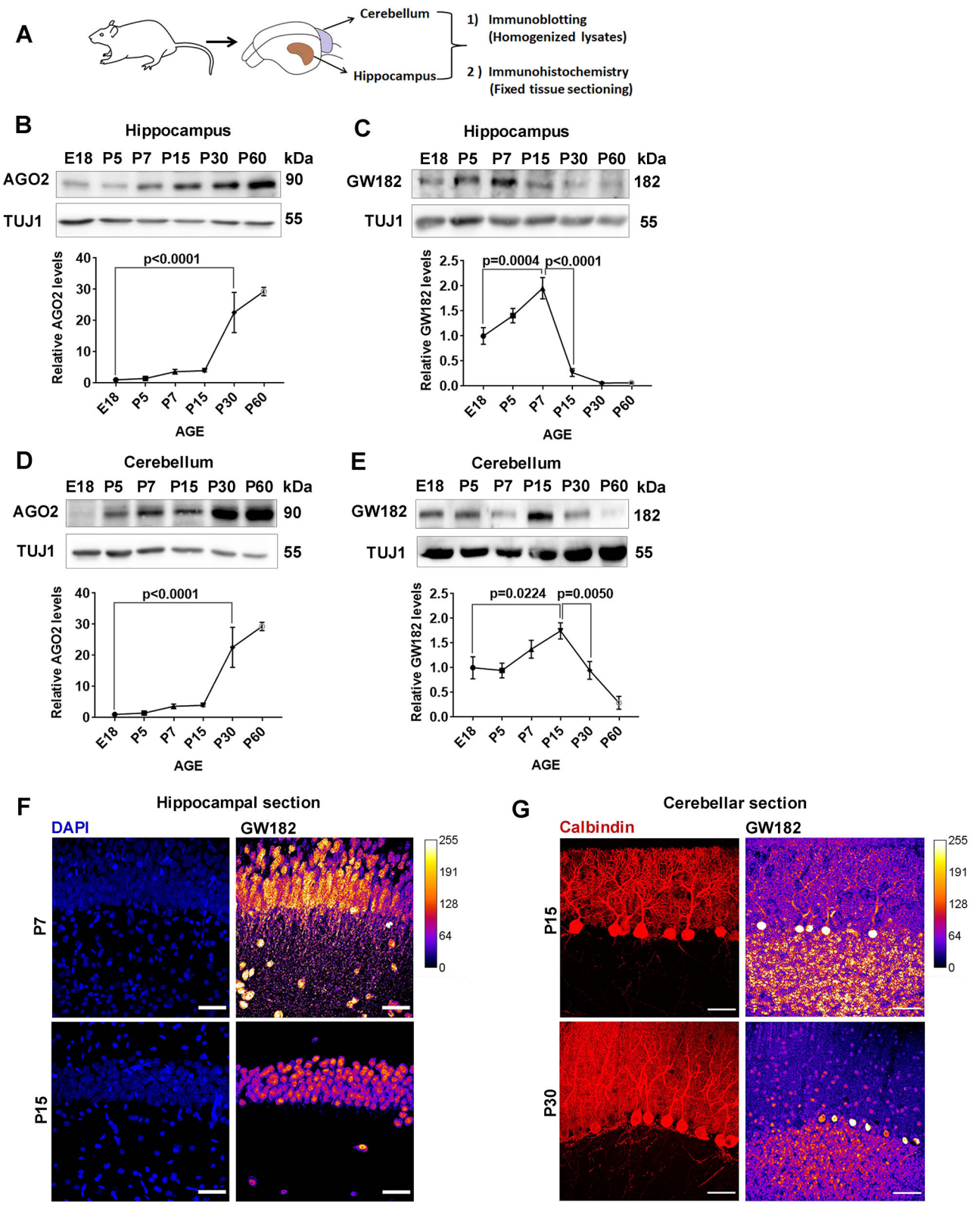

Fig. 1. See next page for legend.

Our analyses of GW182 expression show that expression peaks during the period of extensive dendrite growth, and that GW182 levels begin to drop when the neurons become primed to respond to neuronal activity (beginning of synaptogenesis). We hypothesized that the increase in neuronal activity during this developmental period drives the reduction in GW182 expression. To test this, DIV7 neuronal cultures were chronically treated with either picrotoxin, to increase neuronal activity, or tetradotoxin (TTX) for suppression of neuronal activity (Fig. 2G). We validated the effects of TTX treatment by quantifying levels of ERK (ERK1 and ERK2, also known as

Journal of Cell Science (2021) 134, jcs258465. doi:10.1242/jcs.258465

Fig. 1. GW182 expression is developmentally regulated in rodent brain. (A) Schematic showing the experimental procedure used to assess the expression pattern of miRISC proteins in rodent brain. (B) Representative immunoblots (top) and line graph (bottom) depicting AGO2 expression profile during hippocampal development. Data represent mean±s.e.m. relative AGO2 levels normalized to TUJ1. *n*=3–5 animals per group. One-way ANOVA with Bonferroni's multiple comparisons test. (C) Representative immunoblots (top) and line graph (bottom) depicting GW182 expression profile during hippocampal development. Data represent mean±s.e.m. relative GW182 levels normalized to TUJ1. *n*=3–5 animals per group. One-way ANOVA with Bonferroni's multiple comparisons test. (D) Representative immunoblots (top) and line graph (bottom) depicting AGO2 expression profile during cerebellar development. Data represent mean±s.e.m. relative AGO2 levels normalized to TUJ1. *n*=3–5 animals per group. One-way ANOVA with Bonferroni's multiple comparisons test. (E) Representative immunoblots (top) and line graph (bottom) depicting GW182 expression profile during cerebellar development. Data represent mean±s.e.m. relative GW182 levels normalized to TUJ1. *n*=3–5 animals per group. One-way ANOVA with Bonferroni's multiple comparisons test. (F) Representative immunohistochemistry images showing DAPI and GW182 staining in rat hippocampal CA1 region at P7 and P15. (G) Representative immunohistochemistry images showing calbindin and GW182 staining in rat cerebellar sections at P15 and P30. Images in F and G are representative of *n*=3–5 experiments. Color scale for GW182 staining represents fluorescence intensity. Scale bars: 50 µm.

MAPK3 and MAPK1) phosphorylation. In accordance with previous reports (Bateup et al., 2013), we observed over 50% reduction in ERK phosphorylation after 24 h of TTX treatment (Fig. 2H,I). When we tested the effect of TTX treatment on GW182 levels, we found that 48 h of TTX treatment resulted in over 2-fold increase in GW182 protein levels (Fig. 2J). GW182 mRNA also showed a similar trend of increase (although not significant) in response to TTX treatment (Fig. S2A). Conversely, increased ERK phosphorylation (24 h) was used to validate picrotoxin treatment (Fig. 2K,L). We observed ∼40% reduction in GW182 levels upon 48 h of picrotoxin treatment (Fig. 2M). The reduced expression of GW182 upon picrotoxin treatment observed at the protein level was also seen at the mRNA level (Fig. S2B). In summary, we found that GW182 levels are inversely regulated by neuronal activity. Taken together, these results establish the recapitulation of the GW182 expression pattern in dissociated neuronal cultures. Furthermore, we verify the role of neuronal activity in the regulation of GW182 expression.

Loss of GW182 function reduces the complexity of dendritic arbors

The developmentally controlled expression and dendritic localization of GW182 indicate a possible role in the regulation of dendritic arborization. To address this, we utilized a loss-of-function approach. We used a GFP-tagged dominant-negative mutant of GW182 (DNGW182) to perturb GW182 function (Jakymiw et al., 2005) during a period of rapid dendritogenesis (DIV3–DIV7) in cultured neurons. GW182 is a scaffolding protein that consists of an N-terminal AGO-binding domain and a C-terminal silencing domain. The dominant-negative mutant lacks the silencing domain and hence cannot function in the canonical miRNA pathway (Jakymiw et al., 2005).

The expression of DNGW182 was verified in HEK 293T cells using immunoblotting and immunostaining analysis (Fig. S4A,C). DNGW182 was observed as a band of ∼85 kDa on western blots probed with an anti-GFP antibody (Fig. S4A). Immunostaining analysis revealed a diffuse expression pattern of DNGW182, in contrast to that of overexpressed full-length GW182, which showed punctate distribution (Fig. S4C). We also examined the expression pattern of DNGW182 in neurons and observed a diffuse expression pattern similar to that observed in HEK 293T cells (Fig. S4D). Previously, it has been reported that DNGW182 exerts dominant-negative effects via the disassembly of P-bodies and sequestration of AGO2 (Jakymiw et al., 2005). To further understand whether DNGW182 causes any changes in the localization of endogenous AGO2, we examined the effect of DNGW182 overexpression on AGO2 puncta localization. To this end, we overexpressed the GFP-tagged DNGW182 or GFP-tagged GW182 in HEK 293T cells and performed AGO2 staining 24 h post transfection (Fig. S4E). We measured different properties of AGO2 localization, including normalized puncta intensity and puncta area. We did not observe any significant difference in these parameters between cells transfected with GFP-tagged GW182 or GFP-tagged DNGW182 (Fig. S4F,G), indicating that DNGW182 does not cause any changes in the localization of endogenous AGO2. After initial validation, we overexpressed GFP-tagged DNGW182 in primary hippocampal neurons on DIV3 and assessed the effect on dendritic arborization on DIV7 (Fig. S3A). Neurons were selected based on GFP staining, and dendrites were identified using MAP2 immunostaining. Neurons overexpressing the GFP construct (without DNGW182) were used as a control. We used Sholl analysis to study dendrite arborization and NeuronJ neurite-tracing software (Meijering et al., 2004) to quantify the dendrite length. Neurons overexpressing DNGW182 showed significantly reduced dendritic intersections at a distance of 8–64 µm from the soma in the sholl profile, indicating a less complex dendritic arbor (Fig. S3B,C). We found a reduced number of total dendritic intersections, as well as a reduction in total dendritic length and length of longest dendrite, in neurons overexpressing DNGW182 (Fig. S3D–F). In summary, perturbation of GW182 function using DNGW182 results in reduced complexity of dendritic arborization.

Next, we questioned whether GW182 regulates dendritic morphology during later stages of dendritic development as well. To address this, we transfected DIV7 hippocampal neurons with GFP or GFP-tagged DNGW182 and fixed the neurons on DIV11 for evaluation of dendritic morphology (Fig. S3G). At this stage, overexpression of DNGW182 did not cause any change in dendritic morphology, as depicted by the Sholl profile (Fig. S3H,I), the total number of dendritic intersections and total dendritic length (Fig. S3J,K). These results suggest that GW182 regulates dendritic growth only during a restricted temporal window.

Multiple studies have demonstrated the importance of BDNF in the regulation of dendrite arborization (Gorski et al., 2003; McAllister et al., 1996). Here, we examined whether perturbation of GW182 function affects BDNF-induced dendritic growth in cultured neurons. Neurons were transfected with either GFP or GFP-tagged DNGW182 on DIV3 followed by 48 h BDNF (50 ng/ml) treatment from DIV5 to DIV7. The neurons were fixed on DIV7, followed by immunostaining (Fig. S3L). In GFP-transfected neurons, BDNF stimulation resulted in enhanced dendrite arborization, as demonstrated by the Sholl profile (Fig. S3M,N). Furthermore, BDNF treatment resulted in an increase in total dendritic length and total intersections in GFP-transfected neurons (Fig. S3O,P). This validated the biological response to BDNF treatment in our system. When the BDNF response was measured in DNGW182-transfected neurons, we found that these neurons were still responsive to BDNF stimulation (Fig. S3M–P). Similar to the effects on GFP-transfected neurons, BDNF treatment increased the dendritic arborization and length of DNGW182-transfected neurons as well (Fig. S3N–P). These results indicate that GW182 does not modulate BDNF-induced dendritic growth in DIV3–DIV7 neurons.

As an independent loss-of-function approach, we used siRNA against GW182 to demonstrate the role of GW182 in the regulation

Journal of Cell Science (2021) 134, jcs258465. doi:10.1242/jcs.258465

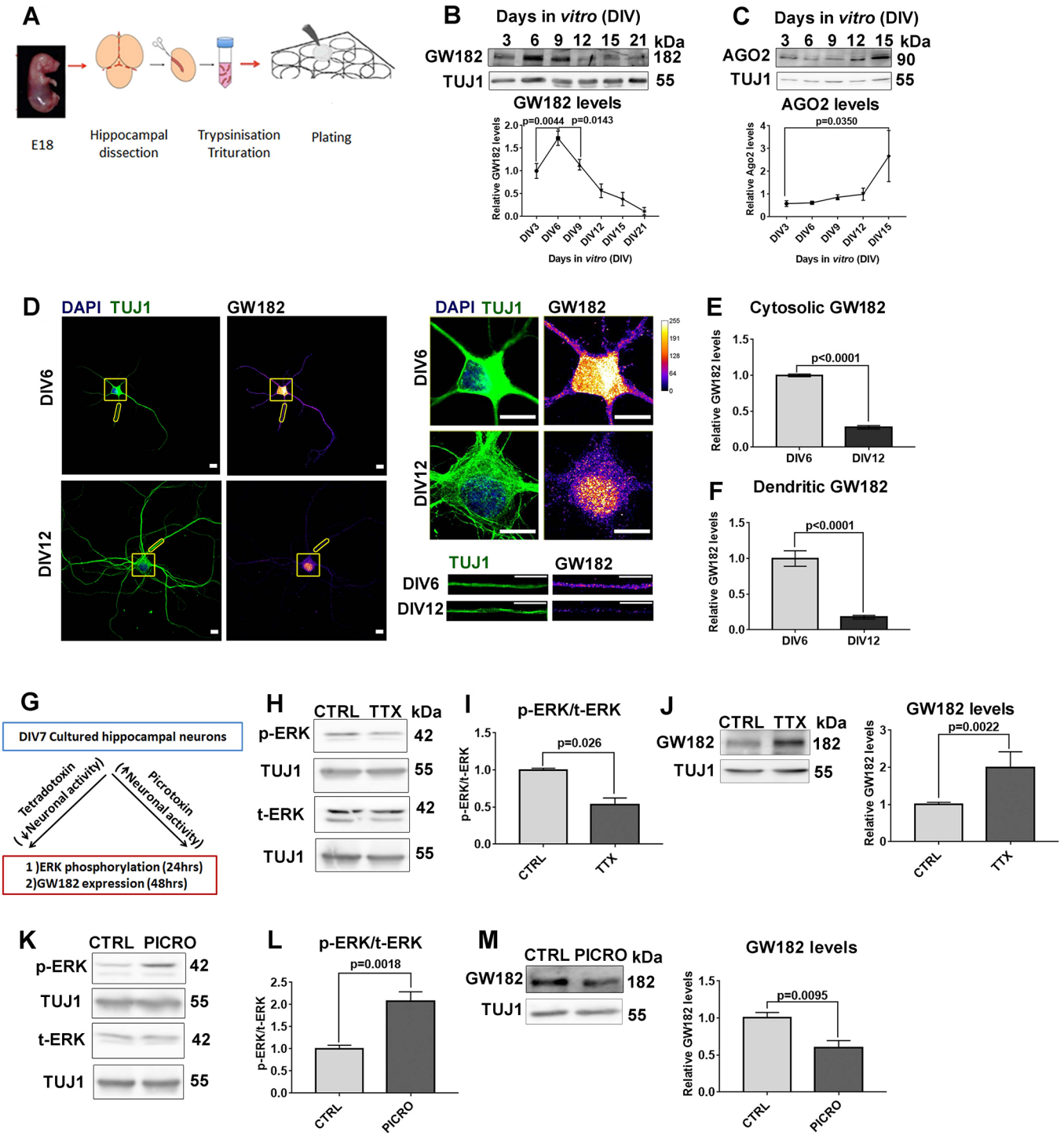

Fig. 2. See next page for legend.

of dendritic morphology. The siRNA-mediated knockdown of GW182 was validated using immunoblotting in Neuro2A cells. GW182 siRNA-transfected cells showed ∼70% reduction in GW182 protein levels as compared to levels in scrambled siRNA-transfected cells (Fig. S3Q). We also validated GW182 knockdown in cultured neurons using immunoblotting and immunolabeling techniques (Fig. S3R,S). In cultured neurons, GW182 siRNA transfection resulted in ∼30% reduction in total GW182 levels as compared to the levels in cells transfected with scrambled siRNA (Fig. S3R), as measured using quantitative immunoblotting. To validate the siRNA-mediated knockdown of GW182 using immunostaining, we co-transfected cultured neurons with GFP along with scrambled or GW182 siRNA at DIV3. The transfected neurons were fixed at DIV5, and the amount of GW182 was measured using immunostaining in GFP-transfected neurons (Fig. S3S). We found that the GFP- and GW182 siRNA-transfected group showed an average of 40% reduction in GW182 levels as compared to levels in the GFP- and scrambled

Fig. 2. Spatiotemporal expression pattern of GW182 in cultured hippocampal neurons. (A) Schematic representing the procedure for embryonic hippocampal neuronal culture. (B) Representative immunoblots (top) and line graph depicting GW182 expression profile in hippocampal neuronal culture from DIV3 to DIV21. Data represent mean±s.e.m. relative GW182 levels normalized to TUJ1. *n*=4–6 independent experiments. One-way ANOVA with Bonferroni's multiple comparisons test. (C) Representative immunoblots (top) and line graph depicting AGO2 expression profile in hippocampal neuronal culture from DIV3 to DIV15. Data represent mean±s.e.m. relative AGO2 levels normalized to TUJ1. *n*=3–5 independent experiments. One-way ANOVA with Bonferroni's multiple comparisons test. (D) Representative images showing DAPI, TUJ1 and GW182 immunostaining in cultured neurons at DIV 6 and DIV12 (left), along with enlarged images of a section of the cell body (right, top; regions marked by square boxes in left-hand images) and dendrites (right, bottom; regions marked by rectangular boxes in left-hand images). Color scale for GW182 staining represents fluorescence intensity. Scale bars: 10 µm. (E) Quantification of mean±s.e.m. normalized mean fluorescence intensity of cytosolic GW182 levels in DIV6 and DIV12 neurons. *n*=27–32 neurons from four independent experiments. Two-tailed unpaired *t*-test. (F) Quantification of mean±s.e.m. normalized mean fluorescence intensity of dendritic GW182 levels in DIV6 and DIV12 neurons. *n*=27–32 neurons from four independent experiments. Two-tailed unpaired *t*-test. (G) Schematic representing the picrotoxin or TTX treatment protocol in cultured neurons. (H) Representative immunoblots depicting ERK phosphorylation status at 24 h post TTX treatment of DIV7 neuronal culture (CTRL, control untreated neurons; p-ERK, phosphorylated ERK; t-ERK, total ERK). TUJ1 is shown as a loading control. (I) Quantification of ERK phosphorylation after 24 h TTX treatment of DIV7 neuronal culture. Data represent the mean±s.e.m. ratio of p-ERK to t-ERK. ERK levels are normalized to TUJ1. *n*=3–5 independent experiments. Two-tailed unpaired *t*-test. (J) Representative immunoblots (left) and corresponding quantification (right) depicting GW182 levels 48 h post TTX treatment in neuronal culture. Data represent mean±s.e.m. relative GW182 levels normalized to TUJ1. *n*=3–5 independent experiments, Two-tailed unpaired *t*-test. (K) Representative immunoblots depicting ERK phosphorylation post 24 h picrotoxin treatment (PICRO) of DIV7 neurons. TUJ1 is shown as a loading control. Molecular mass is indicated in kDa. (L) Quantification of ERK phosphorylation after 24 h picrotoxin treatment of DIV7 neuronal culture. Data represent the mean±s.e.m. ratio of p-ERK to t-ERK normalized to TUJ1. *n*=3–5 independent experiments. Two-tailed unpaired *t*-test. (M) Representative immunoblots (left) and corresponding quantification (right) depicting GW182 levels post 48 h picrotoxin treatment in neuronal culture. Data represent mean±s.e.m. relative GW182 levels normalized to TUJ1. *n*=3–5 independent experiments. Two-tailed unpaired *t*-test.

siRNA-transfected group (Fig. S3S,T). The relatively lower knockdown efficiency in cultured neurons is potentially due to the inclusion of GFP-transfected neurons that were not co-transfected with GW182 siRNA in the averaged quantification data. To study the effect of GW182 knockdown on dendrite arborization, cultured hippocampal neurons were transfected with GFP along with scrambled or GW182 siRNA on DIV3, followed by fixation and immunostaining on DIV7 (Fig. 3A). Similar to the phenotype observed with DNGW182, we found that siRNA-mediated knockdown of GW182 resulted in a reduced number of dendritic intersections in the Sholl curve, indicating a reduction in dendrite arborization (Fig. 3B,C). Moreover, neurons transfected with GW182 siRNA showed ∼20% reduction in the total dendritic length and total number of intersections, as compared to those of scrambled siRNA-transfected neurons (Fig. 3D; Fig. S3U). However, unlike DNGW182-transfected neurons, we did not observe any difference in the length of the longest dendrite between scrambled siRNA- and GW182 siRNA-transfected neurons (Fig. S3V). We also addressed the effect of GW182 knockdown in cultured neurons during later stages of dendritic development (DIV7–DIV11; Fig. 3E). At this stage, we did not observe any difference in the dendritic morphology between GW182 siRNA- and scrambled siRNA-transfected neurons (Fig. 3F,G). The neurons showed a similar number of dendritic intersections as well as similar total dendritic length (Fig. 3H; Fig. S3W). Taken together, these results show that the loss of GW182 function results in reduced dendritic arborization and total dendritic length during a restricted temporal window of dendritic development.

GW182 overexpression potentiates dendritic growth and arborization

In the above section, we used a loss-of-function method to demonstrate the role of GW182 in the regulation of dendritic morphology. To further strengthen our findings, we employed a gain-of-function approach involving overexpression of full-length GW182. The overexpression of GFP-tagged GW182 was validated in HEK 293T cells and cultured hippocampal neurons (Fig. S4B–D). In HEK 293T cells, GFP-tagged GW182 was observed in western blots as a band of ∼210 kDa that could be detected by both anti-GFP and anti-GW182 antibodies (Fig. S4B). In both HEK 293T cells and cultured neurons, GFP-tagged GW182 overexpression gave punctate staining (Fig. S4C,D). To study the effect of GW182 overexpression on dendritic arborization, we transfected cultured hippocampal neurons on DIV3 with either GFP or GFP-tagged GW182, followed by fixation and immunostaining at DIV7 (Fig. 4A). Sholl analyses indicated an increase in dendritic branching in GW182-overexpressing neurons as compared to that of GFP-transfected neurons (Fig. 4B,C). GW182 overexpression resulted in a 2-fold increase in total dendritic length, as well as an increase in the total number of dendritic intersections (Fig. 4D; Fig. S4H). Hence, overexpression of GW182 promotes dendritic growth arborization and has an opposite effect on dendritic arborization compared to GW182 knockdown. Collectively, these experiments demonstrate the permissive role of GW182 in the regulation of dendrite morphology.

GW182 regulates somatodendritic translation in developing neurons

We next sought to identify the molecular mechanism of GW182-mediated regulation of dendritic growth. Several studies have demonstrated the importance of protein synthesis and various RBPs in the regulation of diverse aspects of dendrite morphogenesis (Bestman and Cline, 2008; Chihara et al., 2007; Perycz et al., 2011; Ye et al., 2004). Furthermore, multiple studies have also implicated GW182 in translational silencing (Yao et al., 2011). Based on the above information, we wanted to investigate the role of GW182 in the regulation of neuronal translation. We monitored neuronal translation using the FUNCAT metabolic labeling technique, which has been described previously (Dieck et al., 2012; Dieterich et al., 2010). FUNCAT is a click-chemistry-based approach to study the spatiotemporal pattern of protein synthesis in cells. Here, the cellular medium containing methionine is replaced with an azide-bearing methionine analog such as L-azidohomoalanine (AHA). During active translation, the provided AHA is incorporated into newly synthesized proteins, which can then be visualized by attaching an alkyne-bearing fluorophore to the amine group of AHA in a copper-catalyzed click-chemistry reaction. The reduction in the FUNCAT signal of neurons incubated with the protein synthesis inhibitor anisomycin verified that the signal can be specifically attributed to proteins synthesized during the labeling period (Fig. S5A). First, we examined the changes in global somatodendritic translation in neurons during neuronal development. For this, we performed FUNCAT labeling at different stages of neuronal development in culture neurons, from DIV3 to

Journal of Cell Science (2021) 134, jcs258465. doi:10.1242/jcs.258465

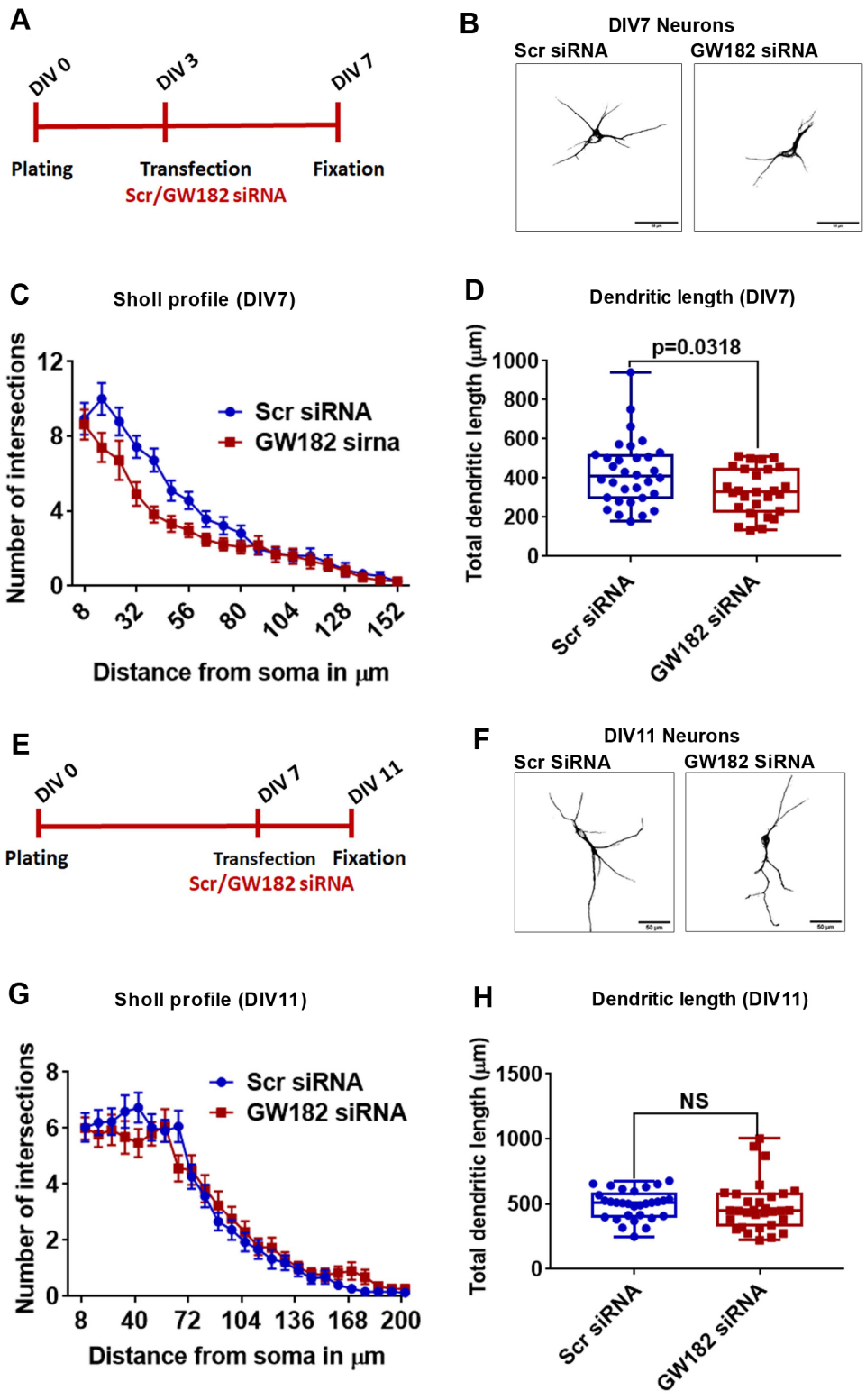

Fig. 3. Loss of GW182 function leads to a reduction in dendritic arborization of hippocampal neurons. (A) Schematic showing the experimental procedure and timeline. Cultured neurons were transfected with either scrambled (Scr) or GW182 siRNA along with GFP on DIV3 and fixed on DIV7, followed by immunostaining. (B) Representative micrographs of DIV7 cultured neurons transfected with either scrambled or GW182 siRNA. Scale bars: 50 µm. (C) Sholl curve of DIV7 cultured neurons transfected with either scrambled or GW182 siRNA on DIV3. Data are mean±s.e.m., *n*=32 neurons from four independent experiments. GW182 siRNA-transfected neurons had significantly more dendritic intersections than scrambled siRNA-transfected neurons at 16–40 µm from the soma (two-way ANOVA with Bonferroni's multiple comparisons test). (D) Quantification of the total dendritic length of DIV7 neurons transfected with either scrambled or GW182 siRNA on DIV3. *n*=27–32 neurons from four independent cultures. Mann–Whitney test. (E) Schematic showing the experimental procedure and timeline. Cultured neurons were transfected with either scrambled or GW182 siRNA along with GFP on DIV7 and fixed on DIV11. (F) Representative micrographs of DIV11 hippocampal neurons transfected with either scrambled or GW182 siRNA on DIV7. Scale bars: 50 µm. (G) Sholl curve of DIV11 cultured hippocampal neurons transfected with either Scrambled or GW182 siRNA on DIV7. Data are mean±s.e.m., *n*=30 neurons from four independent experiments. (H) Quantification of the total dendritic length of DIV11 hippocampal neurons transfected with either scrambled or GW182 siRNA on DIV7. *n*=30 neurons from four independent cultures. Mann–Whitney test (NS, not significant). In D and H, boxes show the interquartile range, the median is marked by a line and whiskers show the range.

DIV12 (Fig. S5B). We observed an overall 70% reduction in FUNCAT signals between DIV6 and DIV9 (Fig. S5B). The FUNCAT signal remained low from DIV9 onwards. This showed us that overall neuronal translation reduces with neuronal development. Next, we wanted to investigate the effect of GW182 on neuronal translation at a stage where both GW182 levels and neuronal translation are optimal. As reported above, the level of GW182 and translation starts to decline after DIV6, and alterations in GW182 expression at DIV3 result in dendritic morphology changes at DIV7. We thereby reasoned that GW182 might regulate neuronal translation at an earlier time point to influence dendrite morphology at DIV7. Therefore, we either transfected neurons with GW182 siRNA or scrambled siRNA to test the effect of GW182 knockdown, or overexpressed GFP, GFP-tagged GW182 or GFP-tagged DNGW182

Journal of Cell Science (2021) 134, jcs258465. doi:10.1242/jcs.258465

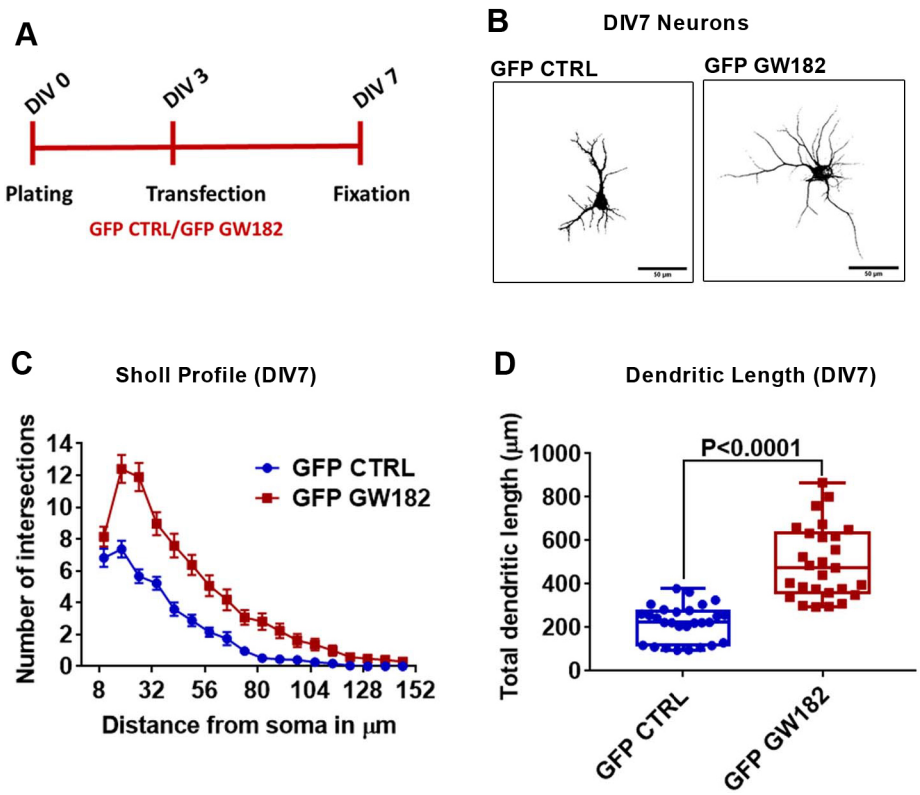

Fig. 4. GW182 overexpression enhances dendrite growth and arborization of hippocampal neurons. (A) Schematic showing the experimental procedure and timeline. Cultured neurons were transfected with GFP (GFP CTRL) or GFP-tagged GW182 (GFP GW182) at DIV3 and fixed at DIV7, followed by immunostaining. (B) Representative micrographs of DIV7 neurons transfected with GFP or GFP-tagged GW182. Scale bars: 50 µm. (C) Sholl curve of DIV7 neurons transfected with GFP or GFP-tagged GW182. Data are mean±s.e.m., *n*=27 neurons from three independent experiments. Neurons overexpressing GFP-tagged GW182 had significantly more dendritic intersections than GFP-overexpressing neurons at 18–82 µm from the soma (two-way ANOVA with Bonferroni's multiple comparisons test). (D) Quantification of the total dendritic length of DIV7 hippocampal neurons transfected with vectors to express either GFP or GFP-tagged GW182. *n*=27 neurons from three independent cultures. Boxes show the interquartile range, the median is marked by a line and whiskers show the range. Two-tailed unpaired *t*-test with Welch's correction.

at DIV3, followed by assessment of neuronal translation at DIV5 or DIV6 (Fig. 5A). We found that GW182 knockdown resulted in over 50% increase in somatodendritic FUNCAT intensity of neurons at DIV5 (Fig. 5B,C). However, when we examined the effect of GW182 knockdown in neurons at DIV6, we did not observe any significant difference in the somatodendritic FUNCAT signal (Fig. S5C). Conversely, GW182-overexpressing neurons showed ∼70% reduction in somatodendritic FUNCAT intensity at DIV5 (Fig. 5D,E).

In addition, we tested the effect of DNGW182 on neuronal translation. In our morphology experiments, we found that DNGW182 influenced dendritic morphology in a similar manner to GW182 knockdown (Fig. 3; Fig. S3). Surprisingly, we found that in contrast to increased FUNCAT signal in GW182-knockdown cells, overexpression of DNGW182 resulted in reduced somatodendritic FUNCAT signal in cultured neurons at DIV5 and DIV6 (Fig. S5D,E). This indicates that overexpression of DNGW182 is not the same as knockdown of GW182 with respect to translation response. Overall, we found that GW182 downregulates global translation in the somatodendritic compartment of developing neurons.

GW182 is a crucial regulator of dendritic F-actin and LIMK1 levels

In the experiments described above, we established the role of GW182 in the regulation of protein synthesis and dendritic arborization. Since cytoskeletal remodeling is a fundamental determinant of dendritic arborization, we hypothesized that GW182 might impact dendritic architecture via regulation of the neuronal cytoskeleton (Jan and Jan, 2010). Both actin and microtubule elements play an essential role in determining the dendritic architecture. Here, we focused on whether GW182 regulates dendritic actin dynamics. Actin is known to exist in two states: the monomeric G-actin, which polymerizes to form asymmetric two-stranded helical F-actin. Actin polymerization dynamics (such as actin treadmilling and changes in F-actin:G-actin ratio) regulate distinct features of dendritic morphology (Georges et al., 2008; Ravindran et al., 2019; Wolterhoff et al., 2020). Here, we determined the influence of GW182 expression on dendritic F-actin levels. We measured the amount of dendritic F-actin using phalloidin staining. GW182 expression was modified by transfecting the neurons with scrambled siRNA or GW182 siRNA, or with GFP, GFP-tagged GW182 or GFP-tagged DNGW182 at DIV3, followed by fixation of the neurons at DIV7 and staining with phalloidin and anti-MAP2 antibody (Fig. 6A). Neurons transfected with GW182 siRNA demonstrated significantly increased levels of dendritic F-actin (Fig. 6B,C). Conversely, neurons overexpressing GFP-tagged GW182 showed reduced F-actin levels in the dendrites (Fig. 6D,E). Surprisingly, upon overexpression of DNGW182, we did not see any change in the dendritic F-actin levels (Fig. S6A,B). The opposite effects of knockdown and overexpression of GW182 on dendritic F-actin levels indicate that GW182 has an important role in determining dendritic actin dynamics.

We next sought to identify the mechanism behind GW182-mediated regulation of dendritic F-actin levels. Multiple actin-binding proteins cooperate to control the structure and stability of the neuronal actin network (Jan and Jan, 2010). Among these, LIMK1 acts as a key regulatory protein and is known to control dendritic morphology via regulation of actin polymerization (Ravindran et al., 2019; Saito et al., 2013). Furthermore, LIMK1 is translationally regulated in neurons downstream of external cues and is also regulated by the miRNA machinery (Ravindran et al., 2019; Schratt et al., 2006). We investigated whether an alteration in GW182 levels influences LIMK1 expression. To address this, we employed a loss-of-function approach. We performed GW182 knockdown in cultured hippocampal neurons at DIV3 by transfecting the neurons with scrambled siRNA or GW182 siRNA along with GFP. The transfected neurons were fixed at

Journal of Cell Science (2021) 134, jcs258465. doi:10.1242/jcs.258465

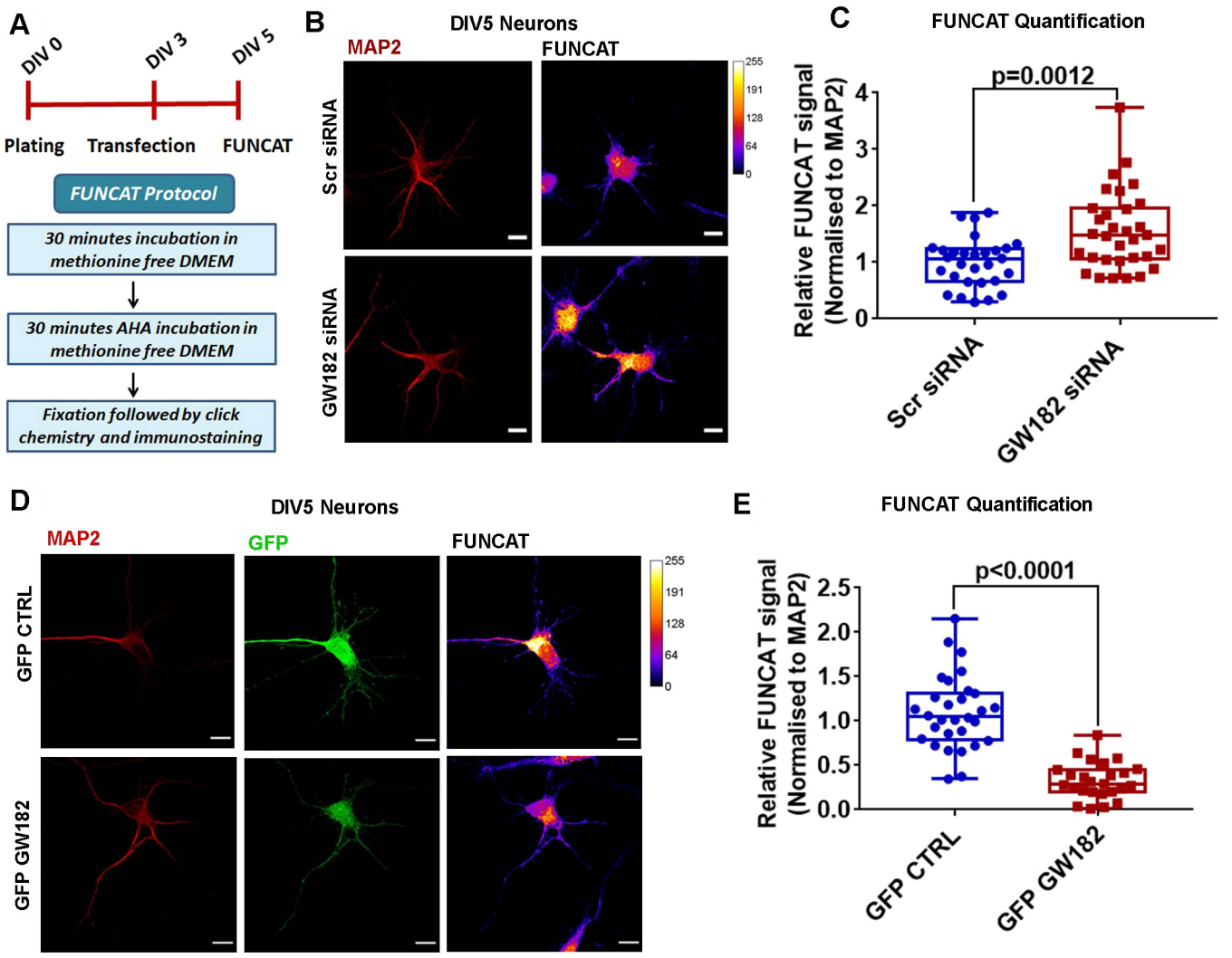

Fig. 5. GW182 regulates global translation in developing neurons. (A) Schematic showing the experimental procedure and timeline to visualize and quantify global protein synthesis in DIV5 cultured neurons using FUNCAT. (B) Representative images of DIV5 cultured neurons showing FUNCAT signal and MAP2 staining in scrambled siRNA (Scr)- or GW182 siRNA-transfected neurons. Color scale for FUNCAT staining represents fluorescence intensity. Scale bars: 10 µm. (C) Quantification of normalized FUNCAT signal (normalized to corresponding MAP2 signal) in scrambled siRNA- or GW182 siRNA-transfected neurons. *n*=29–32 neurons from four independent experiments. Mann–Whitney test. (D) Representative images of DIV5 cultured neurons showing FUNCAT signal in control GFP (GFP CTRL)-transfected and GFP-tagged GW182 (GFP GW182)-transfected neurons. GFP signal and MAP2 staining are also shown. Color scale for FUNCAT staining represents fluorescence intensity. Scale bars: 10 µm. (E) Quantification of FUNCAT signal (normalized to corresponding MAP2 signal) in control GFP- and GFP GW182-transfected neurons. *n*=25–30 neurons from four independent experiments. Two-tailed unpaired *t*-test with Welch's correction. In C and E, boxes show the interquartile range, the median is marked by a line and whiskers show the range.

DIV7 and examined for levels for LIMK1 using quantitative immunofluorescence. LIMK1 levels were significantly reduced in neurons with GW182 knockdown as compared to levels in the neurons transfected with scrambled siRNA (Fig. 6F,G).

We further validated this result by employing the DNGW182 mutant to perturb GW182 function. We quantified LIMK1 levels in DIV7 neurons transfected with either GFP or GFP-tagged DNGW182 on DIV3 (Fig. S6C). Similar to the effects of GW182 knockdown, perturbation of GW182 function using DNGW182 also led to a significant reduction in somatodendritic LIMK1 levels (Fig. S6C,D). Conversely, overexpression of GW182 led to increased LIMK1 expression in HEK 293T cells (Fig. S6E,F).

Having demonstrated that modulation of GW182 expression results in altered LIMK1 and F-actin levels, we speculated that GW182 regulates dendritic arborization through modulation of LIMK1 expression. If that were the case, knocking down LIMK1 should limit the dendritic overgrowth phenotype caused by GW182 overexpression. LIMK1 siRNA was validated using immunostaining analysis in cultured neurons (Fig. S6G,H). After initial validation of LIMK1 siRNA, to test our hypothesis, we co-transfected DIV3 cultured neurons with scrambled siRNA or LIMK1 siRNA in the background of GFP or GFP-tagged GW182 overexpression (Fig. 6H). These neurons were fixed at DIV7 and immunostained using anti-MAP2 antibody. In agreement with our earlier results, neurons with GFP-tagged GW182 and scrambled siRNA expression showed increased dendritic arborization as compared to neurons with control GFP and scrambled siRNA expression (Fig. 6I,J). In GFP-transfected neurons, knocking down LIMK1 resulted in a significant reduction in dendritic branching and total dendritic length (Fig. 6I–K). Importantly, LIMK1 knockdown partially rescued the dendritic overgrowth phenotype of GW182 overexpression (Fig. 6I,J). We also observed that LIMK1 siRNA transfection

Journal of Cell Science (2021) 134, jcs258465. doi:10.1242/jcs.258465

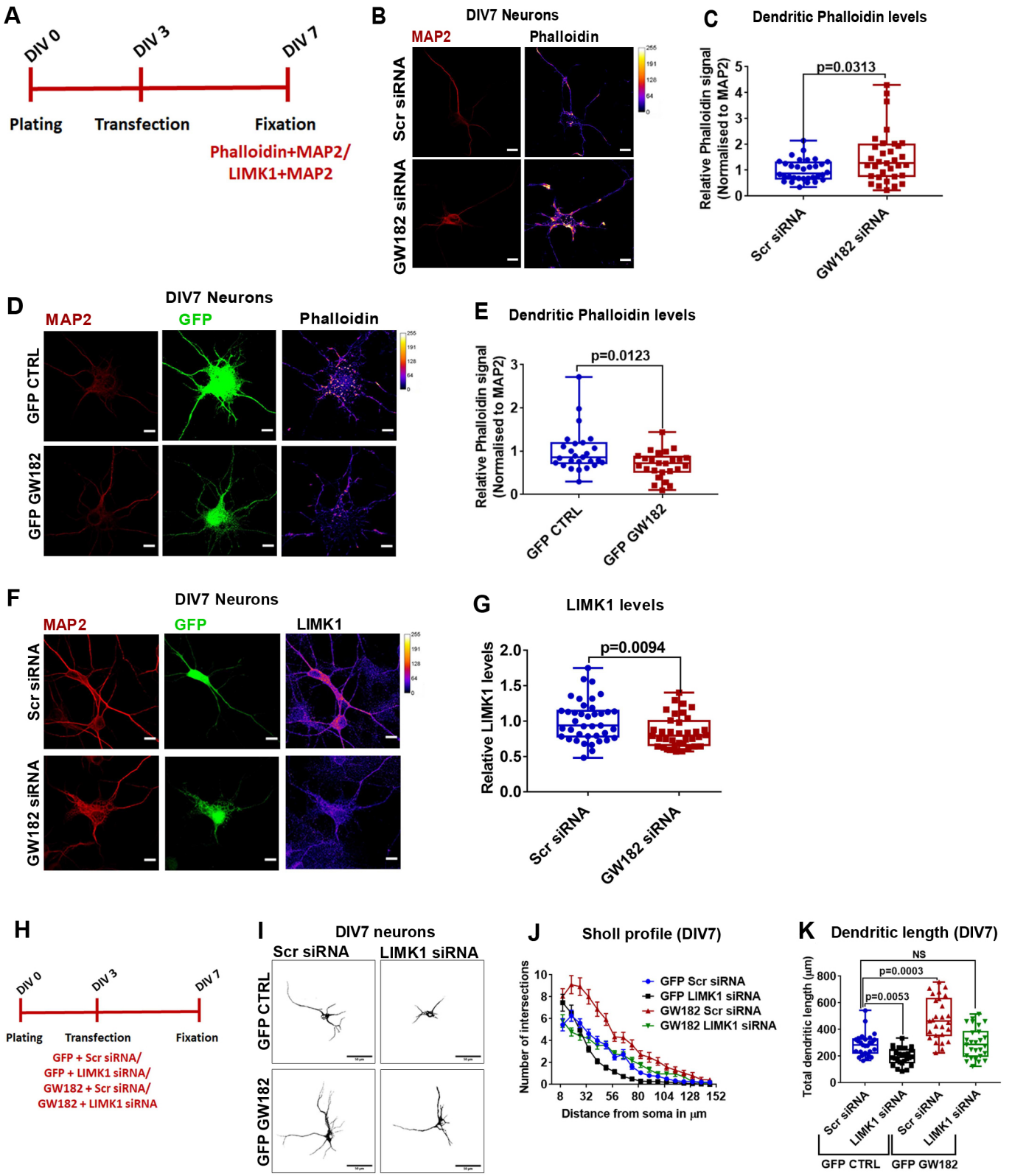

Fig. 6. See next page for legend.

abrogated the GW182-induced increase in total dendrite length and total dendritic intersections (Fig. 6K; Fig. S6I). Taken together, these results suggest that GW182 regulates dendritic morphology via LIMK1-mediated modulation of dendritic actin dynamics (Fig. 7).

DISCUSSION

To date, research on GW182 has primarily focused on understanding its role as an miRISC component. Here, we delineated the role of GW182 in neuronal development. We found

Journal of Cell Science (2021) 134, jcs258465. doi:10.1242/jcs.258465

Fig. 6. GW182 regulates dendritic arborization through LIMK1-mediated modulation of dendritic F-actin levels. (A) Schematic showing the experimental procedure and timeline. Cultured neurons were transfected with expression constructs at DIV3 and fixed at DIV7, followed by MAP2 and phalloidin staining. (B) Representative images of DIV7 cultured neurons showing phalloidin staining in scrambled (Scr) siRNA- or GW182 siRNA-transfected neurons. Color scale for phalloidin staining represents fluorescence intensity. Scale bars: 10 µm. (C) Quantification of phalloidin intensity (normalized to corresponding MAP2 signal) in scrambled siRNA- or GW182 siRNA-transfected neurons. *n*=32–33 neurons from four independent experiments. Mann–Whitney test. (D) Representative images of DIV7 neurons showing phalloidin staining in either GFP control (GFP CTRL)- or GFP-tagged GW182 (GFP GW182)-transfected neurons. MAP2 and GFP signals are shown. Color scale for phalloidin staining represents fluorescence intensity. Scale bars: 10 µm. (E) Quantification of phalloidin intensity (normalized to corresponding MAP2 signal) in GFP CTRL- or GFP GW182-transfected neurons. *n*=25–26 neurons from three independent experiments. Mann–Whitney test. (F) Representative images of DIV7 culture neurons showing LIMK1 staining in scrambled siRNA- or GW182 siRNA-transfected neurons. MAP2 and GFP signals are shown. Color scale for LIMK1 staining represents fluorescence intensity. Scale bars: 10 µm. (G) Quantification of normalized LIMK1 signal in scrambled siRNA- or GW182 siRNA-transfected neurons. *n*=36–39 neurons from four independent experiments. Two-tailed unpaired *t*-test. (H) Schematic showing the experimental procedure and timeline. Cultured neurons were transfected with the indicated expression constructs and siRNAs at DIV3 and fixed at DIV7, followed by MAP2 immunostaining. (I) Representative micrographs of DIV7 cultured hippocampal neurons transfected with control GFP or GFP-tagged GW182 along with scrambled siRNA or LIMK1 siRNA. Scale bars: 50 µm. (J) Sholl curve of DIV7 cultured hippocampal neurons transfected with GFP-tagged GW182 or control GFP along with scrambled siRNA or LIMK1 siRNA. Data are mean±s.e.m., *n*=25–29 neurons from four independent experiments. GFP and LIMK1 siRNA-transfected neurons had significantly fewer dendritic intersections than GFP and scrambled siRNA-transfected neurons at 8 µm and 32–64 µm from the soma. GFP-tagged GW182-overexpressing neurons transfected with scrambled siRNA had significantly more dendrites than GFP-overexpressing neurons transfected with scrambled siRNA at 16–88 µm from the soma. Neurons overexpressing GFP-tagged GW182 and transfected with LIMK1 siRNA had significantly more dendrites than neurons overexpressing GFP and transfected with scrambled siRNA only at 16 µm from the soma. Two-way ANOVA with Bonferroni's multiple comparisons test. (K) Quantification of the total dendritic length of cultured neurons transfected with either control GFP or GFP-tagged GW182 along with scrambled siRNA or LIMK1 siRNA. *n*=26–27 neurons from three independent experiments. Kruskal–Wallis test followed by Dunn's multiple comparisons test (NS, not significant). In C,E,G and K, boxes show the interquartile range, the median is marked by a line and whiskers show the range.

a strictly regulated expression pattern of GW182 during neuronal development, with specific periods of peak expression and decline. Peak GW182 expression coincided with the period of rapid dendritogenesis, followed by reduced GW182 expression in the adult brain. Immunohistochemical analysis of GW182 in hippocampal and cerebellar sections revealed the presence of GW182 in a wide variety of neuronal cells, including glutamatergic (pyramidal and granule cells) as well as GABAergic neurons (Purkinje neurons). During the period of peak expression, GW182 staining was observed in the dendritic region of both hippocampal and cerebellar neuronal populations. Furthermore, later in development, the reduction in GW182 staining was predominantly observed in the cyto-dendritic compartment. Our imaging analysis also revealed substantial staining of GW182 in the neuronal nucleus. As previous studies have indicated an important role for nuclear GW182 in RNA-mediated transcriptional activation (Hicks et al., 2017), it is important to determine the nuclear function of GW182 in neurons.

We observed that the amount of GW182 mRNA remains unchanged during neuronal development, suggesting a role for translation regulatory mechanisms in controlling GW182 levels during neuronal development. However, we cannot rule out the possibility of degradation mechanisms, as previous studies have indicated that GW182 levels can be regulated translationally as well as through ubiquitin-mediated proteasomal degradation (Li et al., 2014; Olejniczak et al., 2016). Our expression profile studies indicate that the developmental reduction in GW182 expression correlates with the emergence of synaptic circuitry and neuronal activity. To elucidate this, we modulated the neuronal activity in hippocampal cultures using TTX and picrotoxin. Application of TTX increased GW182 expression. Conversely, increased neuronal activity using the GABA antagonist picrotoxin resulted in a reduction in GW182 levels. Taken together, these results indicate the potential role of neuronal activity in the regulation of GW182 expression. Previous studies have demonstrated an important role of PI3K–AKT–mTOR and JAK–STAT signaling pathways in regulating the translation of GW182 (La Rocca et al., 2015; Olejniczak et al., 2016). It is important to determine whether these pathways are also involved in neuronal activity-mediated regulation of GW182. Furthermore, it is also important to highlight that even though picrotoxin-mediated changes in neuronal activity resulted in changes in GW182 protein expression similar to those seen upon the emergence of synaptic circuitry during neuronal development, the underlying mechanisms involved in GW182 expression regulation in these two cases are probably distinct. Picrotoxin treatment mimics an accelerated neurodevelopmental event, leading to a reduction in both mRNA and protein levels of GW182, in contrast to the gradual changes during neurodevelopment, which only lead to a decrease in GW182 protein levels, with unchanged mRNA profile. We hypothesize that such changes at both transcriptional and translational levels upon picrotoxin treatment are primarily required for rapid adjustment of GW182 levels in response to increased neuronal activity.

The abundance of GW182 in dendrites during the period of rapid dendritogenesis is suggestive of its role in dendrite morphogenesis. To understand the role of GW182 in dendritic morphogenesis, we perturbed GW182 function during the dendritic growth phase of hippocampal neurons using two independent loss-of-function approaches: siRNA knockdown and expression of the dominant-negative mutant DNGW182. In our study, we performed co-transfection of GFP and GW182 siRNA, and used GFP transfection in neurons as a proxy for transfection of siRNA. However, it is possible that not all the GFP-transfected cells were also transfected with GW182 siRNA, as highlighted by our siRNA validation using immunostaining, where only an average 40% reduction in GW182 expression was seen in GFP-transfected neurons. This is a technical limitation of using a co-transfection method, and a better approach would be to utilize shRNA with GFP expression to achieve knockdown.

Both the knockdown and dominant-negative approaches resulted in the reduction of dendritic arborization. Consistent with this, overexpression of GW182 resulted in increased dendritic arborization. These results establish GW182 as a positive modulator of dendritic growth. We observed that GW182 regulates dendritic arborization only during a specific temporal window, as the loss of GW182 function did not affect dendritic arborization in older neurons (DIV7–DIV11). We hypothesize that this is mainly due to low basal levels of GW182 at this stage. We also observed that perturbation of GW182 function during DIV 3–DIV7 did not affect BDNF-induced dendritic growth. This is in contrast to a previous study suggesting that loss of GW182 prevents BDNF-induced dendritic growth in mature neurons (DIV14; Huang

Journal of Cell Science (2021) 134, jcs258465. doi:10.1242/jcs.258465

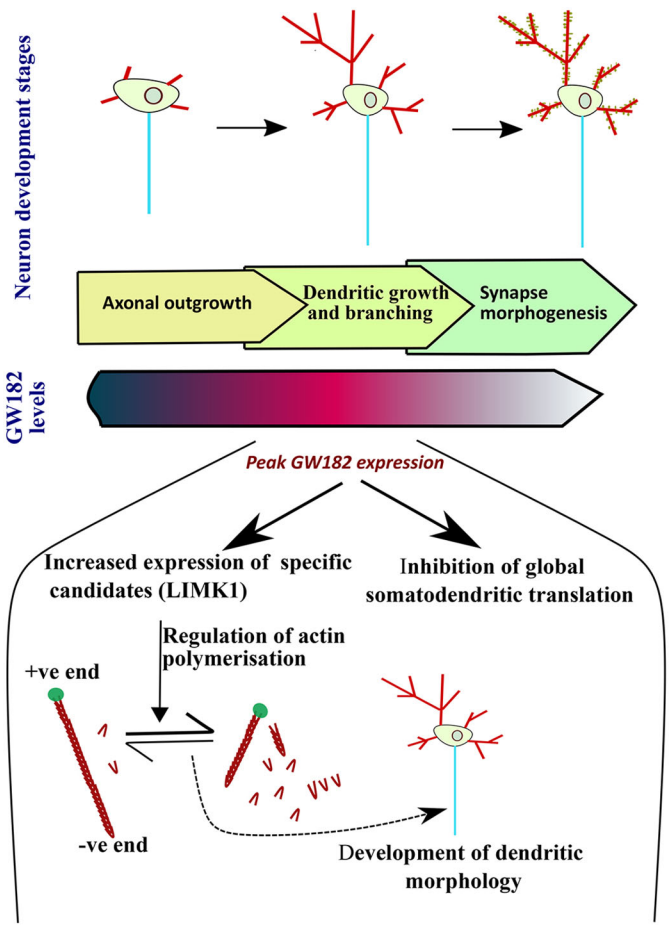

Fig. 7. Model describing GW182-mediated regulation of dendritic arborization. Peak expression of GW182 during the period of rapid dendritogenesis controls dendritic arborization via LIMK1-mediated regulation of actin polymerization.

et al., 2012). We speculate that these contrary findings are primarily due to the differences in the age of neurons and the basal expression of GW182 during the temporal stages examined.

GW182 is likely to regulate dendritic arborization by modulating cytoskeletal elements such as actin and microtubules. Here, we show that GW182 regulates dendritic F-actin levels. Our experiments revealed reduced dendritic F-actin levels in neurons with GW182 overexpression and increased F-actin staining in GW182-knockdown neurons. Although the exact correlation between dendritic F-actin levels and dendritic arborization remains contradictory, substantial evidence has suggested that destabilization of actin filaments in dendrites is required for microtubule invasion of the dendritic filopodia, which in turn leads to branch stabilization and an increase in dendritic length (Poulain and Sobel, 2010; Ravindran et al., 2019). Hence, reduced F-actin levels observed in GW182-overexpressing neurons correlates well with the increased dendritic arborization of these neurons. These experiments establish the actin cytoskeleton as an important player in GW182-mediated dendritic growth. However, at this stage, we cannot rule out the potential contribution of the microtubule cytoskeleton to this regulation.

Previous reports have demonstrated the important role of translation regulation in dendritic morphogenesis (Chihara et al., 2007; Kumar et al., 2005; Lein and Higgins, 1991; Perycz et al., 2011). In most studies, an increase in protein synthesis leads to increased dendritic arborization, and vice versa (Keil et al., 2018; Kumar et al., 2005; Skalecka et al., 2016; Xu et al., 2019). However, in our study, we found a new mechanism where, despite causing disinhibition of global protein synthesis, GW182 knockdown results in reduced dendritic arborization. We speculated that in the background of global translation upregulation, knockdown of GW182 might lead to the downregulation of translation of selective mRNA candidates required for dendritic growth. We identified the actin regulator LIMK1 as one such candidate whose expression is selectively downregulated despite the global translation upregulation observed in GW182-knockdown neurons. Given that previous studies have shown increased miR-134-mediated repression of LIMK1 upon enhancement of AGO–GW182 interaction (Rajgor et al., 2018), the reduction in LIMK1 levels upon GW182 knockdown seems counterintuitive. A possible explanation is that the levels of miR-134 miRNA are reported to be low during the examined developmental stages in our experiment (DIV3–DIV7) (Schratt et al., 2006). Based on this, we hypothesize that the effect of GW182 on LIMK1 may not be mediated directly via miR-134, but indirectly through other regulators of LIMK1 expression. For example, the ubiquitin ligase RNF6 has been shown to be involved in the degradation of LIMK1 in neurons (Tursun et al., 2005). The level of RNF6 is regulated by miR-26a-5P, which has been shown to be predominantly expressed during early neurodevelopment (Huang et al., 2019; Lucci et al., 2020). siRNA-mediated knockdown of GW182 could lead to alleviation of RNF6 repression by miR-26a-5P. The increased RNF6 might target LIMK1 for degradation, explaining the reduced LIMK1 levels observed upon GW182 knockdown.

In accordance with a previous study from our lab, we observed that the dynamic shift in actin polymerization was well correlated with somatodendritic LIMK1 levels upon modulation of GW182 expression (Ravindran et al., 2019). Furthermore, we showed that LIMK1 knockdown abrogated the dendritic overgrowth phenotype of GW182 overexpression. In summary, we have shown that GW182 regulates dendritic arborization via LIMK1-induced changes in the dendritic actin cytoskeleton (Fig. 7). An important direction for future studies is to determine the molecular mechanism of GW182 regulation of LIMK1 expression.

In this study and many previous studies, DNGW182 has been used as a substitute for GW182 knockdown (Huang et al., 2012; Jakymiw et al., 2005). In our dendritic morphology assay, DNGW182 behaved similarly to GW182 knockdown, leading to an overall reduction in dendritic arborization. However, in the FUNCAT assay, unlike the translation upregulation phenotype of GW182 knockdown, overexpression of DNGW182 resulted in translation inhibition. We speculate that DNGW182 causes translation inhibition by sequestering the AGO2–miRNA–mRNA complex irreversibly, thereby preventing mRNA translation. Furthermore, in our experiments involving the measurement of dendritic F-actin levels, expression of DNGW182 did not phenocopy GW182 knockdown. An important question arising from this data is how the DNGW182 mutant still appears to phenocopy GW182 knockdown in terms of dendritic morphology. We speculate that, although upon gross evaluation the dendritic morphology of GW182-knockdown and DNGW182-expressing neurons appears similar, in-depth analysis of dendritic morphology with more refined techniques is required to confidently conclude whether the two indeed yield the same outcome with respect to dendritic arborization. Preliminary indication of the differences in dendritic morphology of DNGW182-expressing and GW182-knockdown neurons came from our analysis of the length of the longest dendrite (Fig. S3F,V), where DNGW182 caused a reduction in the length of the longest dendrite, unlike GW182 knockdown, where the length of the longest dendrite remained unchanged.

Hence, it will be important to acquire an in-depth analysis of dendritic arborization parameters, such as the number and length of primary, secondary and tertiary dendritic branching in GW182-knockdown and DNGW182-transfected neurons, in order to understand the discrepancies associated with the DNGW182 mutant. Furthermore, it is important to emphasize here that the DNGW182 mutant does not behave like GW182 knockdown in every aspect and should be used with caution.

In conclusion, our work has established the crucial role of GW182 in regulating dendritic morphogenesis. As GW182 has recently been implicated in neurodevelopmental disorders as well as Alzheimer's disease (Badhwar et al., 2017; Chen et al., 2019; Eising et al., 2019; Guerrini and Mei, 2018), our work provides a framework for future studies delineating the role of GW182 in different aspects of neuronal development and function. Our study has focused on the GW182 paralog TNRC6A, and hence it will be important to determine whether the other GW182 paralogs, TNRC6B and TNRC6C, play similar roles in neuronal development. This will be primarily dependent on the relative expression of these paralogs at different neurodevelopmental stages and the binding specificity of GW182 paralogs against selected miRNA–mRNA pairs. Another important future direction will be to identify the miRNA candidates involved in GW182-mediated regulation of neuronal development.

MATERIALS AND METHODS

Ethics statement

All animal work was carried out in accordance with the procedures approved by the Institutional Animal Ethics Committee (IAEC) and the Institutional Biosafety Committee (IBSC), InStem, Bangalore, India. All rodent work was done using Sprague Dawley (SD) rats. Rats were kept at 20–22°C with 50–60% relative humidity and 0.3 µm HEPA-filtered air supplied at 15–20 air changes per hour, and a 14 h/10 h light/dark cycle was maintained. Rats were freely supplied with food and water.

Cell lines and primary neuronal culture

Primary neuronal cultures were prepared from the hippocampus of SD rats at embryonic day 18 (E18), as per a previously established procedure (Kaech and Banker, 2006; Ravindran et al., 2019). The dissociated cells were plated at a density of 20,000–30,000 cells/cm^2 on dishes and/or coverslips coated with poly-L-lysine (P2636; Sigma; 0.2 mg/ml in borate buffer, pH 8.5). The neurons were initially plated in Minimum Essential Media (MEM; 10095080; Thermo Fisher Scientific) containing 10% FBS (F2442; Sigma) to aid their attachment. After 3 h, the medium was changed to neurobasal (21103049; Thermo Fisher Scientific) supplemented with B27 (17504044; Thermo Fisher Scientific) and Glutamax (35050-061; Life Technologies). Neurons were cultured for the required time at 37°C in a 5% CO_2 incubator. Transfections were done using Lipofectamine 2000 (11668019; Invitrogen) following a modified manufacturer's protocol. Briefly, 2 µg of DNA or 100 pmol of siRNA was used along with 4 µl of Lipofectamine 2000 per well of a 6-well dish. The cells were incubated in the transfection mixture for 2 h followed by medium change.

HEK 293T and Neuro2A cells were maintained in DMEM (11995; Gibco) with 10% FBS. Cells were cultured for the required time at 37°C in a 5% CO_2 incubator.

Lysate preparation and immunoblotting

Rats of different postnatal ages were euthanized, and the required tissue (hippocampus, cerebellum and liver) was dissected out in cold phosphate-buffered saline (PBS; pH 7.4). The tissue was homogenized in lysis buffer containing 50 mM Tris-HCl pH 7.4, 150 mM NaCl, 5 mM $MgCl_2$ and 0.3% Triton X-100 supplemented with EDTA-free protease inhibitor complex (Sigma; S8830) and phosphatase inhibitor cocktail (04906837001; Roche). The homogenates were centrifuged at 16,000 ***g*** for 30 min at 4°C. Obtained lysates were mixed with 6× Laemmli buffer and were heated at 95°C. The samples were aliquoted and stored at −20°C until further use. Prepared lysates were loaded onto an SDS–PAGE gel and run for 180 min. For experiments involving immunoblotting of GW182, a 6% resolving gel was used. In the rest of the experiments, 8% or 10% resolving gels were used depending upon the molecular mass of proteins to be resolved. Proteins were then transferred to a PVDF membrane (overnight transfer at 20 V or 2 h transfer at 380 mA). Post transfer, the blots were blocked with 5% Blotto (sc2324; Santa Cruz Biotechnology) or 5% BSA (for phospho-antibodies) for 1 h at room temperature. Afterwards, the blots were incubated with the required primary antibody for 3 h at room temperature. The blots were washed with 1% TBST (Tris-buffered saline with 1% Tween 20; GRM156, HIMEDIA) thrice for 10 min each, and incubated with appropriate secondary antibodies for 1 h at room temperature. After subsequent washes with TBST, the blots were developed by a chemiluminescent method using ECL western clarity solution (1705060; Biorad). Images were taken in Image Quant (LAS 4000 or Amersham imager 600). The bands were quantified using ImageJ software (NIH, Bethesda, MD).

RNA extraction and quantitative PCR

Total RNA was extracted from homogenized lysates using Trizol (15596026; Thermo Fisher Scientific), and isolated RNA was converted to cDNA using Superscript III (18080; Invitrogen). Quantitative PCR (qPCR) was performed for the required primers using a Bio-Rad thermal cycler CFX384. Primer sequences are provided in Table S1.

Immunostaining

Rat primary hippocampal neurons were fixed using 4% paraformaldehyde (PFA) for 20 min at room temperature and processed for imaging as described previously (Muddashetty et al., 2011). In brief, cells were permeabilized using TBS_{50} (50 mM Tris-HCl, pH 7.4, and 150 mM NaCl) containing 0.3% Triton X-100. Afterwards, the cells were blocked with blocking buffer (TBS_{50} containing 0.1% Triton X-100, 2% BSA and 2% FBS) for 1 h at room temperature. Neurons were incubated with required antibodies for 2 h at room temperature, followed by washes with TBS_{50} containing 0.1% Triton X-100. After washes, neurons were incubated with suitable secondary antibodies for 1 h at room temperature. After washes, the coverslips were mounted for imaging using Mowiol 4-88 mounting medium. Images were acquired on an FV3000 confocal microscope (Olympus). For neuronal morphology experiments involving Sholl analysis and length measurements, a 40×, NA 1.25, silicon oil immersion objective was used, along with 1 µm step size in the *z* direction. For other experiments involving the quantification of fluorescence intensities, images were taken using a 60×, NA 1.4, oil immersion objective with 0.5 µm step size in the *z* axis. Imaging conditions were kept constant across different datasets in an experiment. In all the experiments, the pinhole was kept at 1 Airy unit.

F-actin measurement

For visualization of F-actin, Alexa Fluor 488 phalloidin (A12379; Invitrogen) was added to the secondary antibody solution (1:50 dilution) during immunostaining and incubated for 1 h. Only the dendritic F-actin levels were measured for intensity calculations. The F-actin levels were quantified as an intensity ratio of phalloidin to MAP2 fluorescence. Image analysis was performed using FIJI software (https://fiji.sc/), and the maximum intensity projection of the slices was used for quantification of the mean fluorescence intensities. The mean fluorescence intensity of the dendritic phalloidin signal was normalized to the corresponding MAP2 intensity.

FUNCAT

For metabolic labeling using fluorescent non-canonical amino acid tagging (FUNCAT), cultured hippocampal neurons were incubated in methionine-free DMEM (21013024; Thermo Fisher Scientific) for 30 min. Afterwards, the neurons were treated with L-azidohomoalanine (AHA, 1 µM; 1066100; Click Chemistry tools) for 30 min in methionine-free DMEM. The coverslips were then washed once with PBS and fixed with 4% PFA for 20 min at room temperature. After fixation, the neurons were permeabilized for 10 min with 0.3% Triton X-100 solution prepared in TBS_{50} (pH 7.6).

The permeabilized neurons were blocked in blocking buffer (TBS_{50} containing 0.1% Triton X-100, 2% BSA and 2% FBS) for 1 h. Afterwards, the neurons were subjected to the FUNCAT reaction for 2 h, where the newly-synthesized AHA-incorporated proteins were tagged with an alkyne-fluorophore Alexa Fluor 555 through a click reaction (C10269, CLICK-iT cell reaction buffer kit; Click Chemistry Tools). After three washes with TBS_{50} containing 0.1% Triton X-100, the neurons were immunostained with anti-MAP2 antibody, followed by mounting with Mowiol medium. The cells were imaged on an Olympus FV300 confocal laser scanning inverted microscope with 60× objective. The pinhole was kept at 1 Airy Unit, and the objective was moved in the *z* direction with a step size of 0.5 µm to collect light from the planes above and below the focal plane. Image analysis was performed using FIJI software, and the maximum intensity projection of the slices was used for quantification of the mean fluorescence intensities. The mean fluorescence intensity of the FUNCAT signal was normalized to the MAP2 intensity of the corresponding neuron.

Perfusion and sectioning

SD rats of required postnatal ages were transcardially perfused with 4% PFA. Afterwards, the brain was carefully dissected out of the skull and kept in 4% PFA overnight for post-fixation. Fixed tissue was washed thrice with 0.1 M phosphate buffer and stored at 4°C until sectioning. Sections of 50 µm thickness were obtained from the required brain region using a Leica VT 1200S vibrating blade microtome. The sections were used for further immunohistochemistry as described above.

Image analysis

All the image analysis was done using Fiji software. For quantification of fluorescence intensity, the confocal stacks were collapsed using the maximum intensity projection method, and the mean intensity was quantified from the cells. For analysis of the cytosolic intensity of GW182, the region of interest (ROI) was defined using tubulin staining, and the mean GW182 intensity was measured in the required ROI. The quantification of AGO2 puncta was also performed in the FIJI software using particle analysis. The mean intensity of AGO2 puncta was normalized to the mean intensity of the total AGO2 signal. Similarly, the area occupied by AGO2 puncta was normalized with the total area. For Sholl analysis quantification, the confocal stacks were first collapsed using the maximum intensity projection method. Thereafter, the MAP2 channel of the images was thresholded manually, and this was used for carrying out Sholl analysis using the Sholl plugin in ImageJ. In all analyses, the starting radius was kept as 10 µm with a step size of 8 µm. For measurement of dendritic length, thresholded MAP2 images were traced using the NeuronJ plugin in ImageJ software as described previously (Meijering et al., 2004).

Statistical analysis

Data distribution was tested for normality using the D'Agostino–Pearson test. Depending on the distribution, either parametric or non-parametric tests were used to quantify statistical significance. For groups with less than five data points, we assumed the data to be normally distributed. For comparing two groups, Student's *t*-test (two-tailed, unpaired) was used for normally distributed data with equal variance, Student's *t*-test with Welch's correction was used for normally distributed data with unequal variances, and Mann–Whitney test was used to compare data with non-normal distribution. Multiple group comparisons were made using one-way ANOVA followed by Bonferroni's multiple comparisons test for parametric data and with Kruskal–Wallis along with Dunn's multiple comparison test for non-parametric data. Sholl profiles between two different groups were assessed using two-way ANOVA followed by Bonferroni's multiple comparisons test. *P* values of less than 0.05 were considered statistically significant. Data are represented as mean±s.e.m.

Antibodies, plasmids and other reagents

The following antibodies were used in this study: anti-GW182/TNRC6A (G5922; Sigma), anti-AGO2 (H00027161-MO1; Abnova), anti-FMRP (F4055; Sigma), anti-MAP2 (M9942; Sigma), anti-MOV10 (ab80613; Abcam), anti-calbindin (214005; Synaptic Systems), anti-TUJ1 (T8578; Sigma), anti-XRN1 (SAB4200028; Sigma), anti-LIMK1 (ab81046; Abcam), anti-ERK (9102; Cell Signaling Technologies), anti-p-ERK (9101; Cell Signaling Technologies), anti-GFP (ab6556; Abcam), HRP-conjugated anti-rabbit IgG (A0545; Sigma), HRP-conjugated anti-mouse IgG (31430; Thermo Fisher Scientific), anti-α-tubulin (T9026; Sigma), Alexa Fluor 488-conjugated anti-mouse IgG (A-11059; Thermo Fisher Scientific), Alexa Fluor 555-conjugated anti-rabbit IgG (A-21428; Thermo Fisher Scientific) and Alexa Fluor 647-conjugated anti-mouse IgG (A-21235; Thermo Fisher Scientific). For western blotting, primary antibodies against AGO2, MOV10, FMRP, XRN1, ERK, p-ERK and LIMK1 were used at 1:1000 dilution; primary antibodies against TUJ1, tubulin and GFP were used at 1:5000 dilution; and the anti-GW182 antibody was used at 1:500 dilution. For immunostaining, primary antibodies against GW182 and LIMK1 were used at 1:200 dilution; and primary antibodies against calbindin, GFP, TUJ1 and MAP2 were used at 1:1000 dilution. Knockdown experiments used LIMK1 siRNA (s134717; Thermo Fisher Scientific), GW182/TNRC6A siRNA (s107649; Thermo Fisher Scientific) and control scrambled siRNA (AM4611; Thermo Fisher Scientific). pmyc-GFP-TNRC6A (Addgene 41999, deposited by Kumiko Ui-Tei; RRID: Addgene_ 41999) and GFP-GW182delta1 (Addgene 11592, deposited by Edward Chan; RRID: Addgene_11592) were from Addgene. Tetradotoxin and picrotoxin were obtained from Tocris Biosciences.

Acknowledgements

We are thankful to the Central Imaging and Flow-cytometry Facility (CIFF) and the animal house facility of NCBS-InStem for providing technical support. We extend our gratitude to all the members of the Muddashetty laboratory for invaluable discussions and suggestions.

Competing interests

The authors declare no competing or financial interests.

Author contributions

Conceptualization: B.N., R.S.M.; Methodology: B.N.; Validation: B.N.; Formal analysis: B.N.; Investigation: B.N.; Resources: A.S., S.C., R.S.M.; Writing - original draft: B.N., R.S.M.; Writing - review & editing: B.N., R.S.M.; Supervision: R.S.M.; Funding acquisition: R.S.M.

Funding

The work was funded by a NeuroStem grant (Department of Biotechnology, Ministry of Science and Technology, India; BT/IN/Denmark/07/RSM/2015-2016) and Science and Engineering Research Board grant (EMR/2016/006313) awarded to R.S.M. B.N. was supported by a Council of Scientific and Industrial Research, India (CSIR) JRF-SRF fellowship [09/860(0172)/2015-EMR-1].

Peer review history

The peer review history is available online at https://journals.biologists.com/jcs/article-lookup/doi/10.1242/jcs.258465

References

Arikkath, J. (2012). Molecular mechanisms of dendrite morphogenesis. *Front. Cell. Neurosci* **6**, 61. doi:10.3389/fncel.2012.00061

Badhwar, A., Brown, R., Stanimirovic, D. B., Haqqani, A. S. and Hamel, E. (2017). Proteomic differences in brain vessels of Alzheimer's disease mice: normalization by PPARγ agonist pioglitazone. *J. Cereb. Blood Flow Metab.* **37**, 1120-1136. doi:10.1177/0271678X16655172

Banerjee, S., Neveu, P. and Kosik, K. S. (2009). A coordinated local translational control point at the synapse involving relief from silencing and MOV10 degradation. *Neuron* **64**, 871-884. doi:10.1016/j.neuron.2009.11.023

Bartel, D. P. (2018). Metazoan MicroRNAs. *Cell* **173**, 20-51. doi:10.1016/j.cell.2018.03.006

Bateup, H. S., Denefrio, C. L., Johnson, C. A., Saulnier, J. L. and Sabatini, B. L. (2013). Temporal dynamics of a homeostatic pathway controlling neural network activity. *Front. Mol. Neurosci* **6**, 28. doi:10.3389/fnmol.2013.00028

Bestman, J. E. and Cline, H. T. (2008). The RNA binding protein CPEB regulates dendrite morphogenesis and neuronal circuit assembly in vivo. *Proc. Natl Acad. Sci. USA* **105**, 20494-20499. doi:10.1073/pnas.0806296105

Brechbiel, J. L. and Gavis, E. R. (2008). Spatial regulation of nanos is required for its function in dendrite morphogenesis. *Curr. Biol.* **18**, 745-750. doi:10.1016/j.cub.2008.04.033

Chen, Y.-C., Chang, Y.-W. and Huang, Y.-S. (2019). Dysregulated translation in neurodevelopmental disorders: an overview of autism-risk genes involved in translation. *Dev. Neurobiol.* **79**, 60-74. doi:10.1002/dneu.22653

Chihara, T., Luginbuhl, D. and Luo, L. (2007). Cytoplasmic and mitochondrial protein translation in axonal and dendritic terminal arborization. *Nat. Neurosci.* **10**, 828-837. doi:10.1038/nn1910

Dieck, S. T., Müller, A., Nehring, A., Hinz, F. I., Bartnik, I., Schuman, E. M. and Dieterich, D. C. (2012). Metabolic labeling with noncanonical amino acids and visualization by chemoselective fluorescent tagging. *Curr. Protoc. Cell Biol.* **0 7**, Unit7.11.

Dieterich, D. C., Hodas, J. J. L., Gouzer, G., Shadrin, I. Y., Ngo, J. T., Triller, A., Tirrell, D. A. and Schuman, E. M. (2010). In situ visualization and dynamics of newly synthesized proteins in rat hippocampal neurons. *Nat. Neurosci.* **13**, 897-905. doi:10.1038/nn.2580

Ding, L. and Han, M. (2007). GW182 family proteins are crucial for microRNA-mediated gene silencing. *Trends Cell Biol.* **17**, 411-416. doi:10.1016/j.tcb.2007.06.003

Dong, X., Shen, K. and Bülow, H. E. (2015). Intrinsic and extrinsic mechanisms of dendritic morphogenesis. *Annu. Rev. Physiol* **77**, 271-300. doi:10.1146/annurev-physiol-021014-071746

Duchaine, T. F. and Fabian, M. R. (2019). Mechanistic insights into MicroRNA-mediated gene silencing. *Cold Spring Harb. Perspect Biol.* **11**, a032771. doi:10.1101/cshperspect.a032771

Eising, E., Carrion-Castillo, A., Vino, A., Strand, E. A., Jakielski, K. J., Scerri, T. S., Hildebrand, M. S., Webster, R., Ma, A., Mazoyer, B., et al. (2019). A set of regulatory genes co-expressed in embryonic human brain is implicated in disrupted speech development. *Mol. Psychiatry* **24**, 1065-1078. doi:10.1038/s41380-018-0020-x

Eulalio, A., Huntzinger, E. and Izaurralde, E. (2008). GW182 interaction with Argonaute is essential for miRNA-mediated translational repression and mRNA decay. *Nat. Struct. Mol. Biol.* **15**, 346-353. doi:10.1038/nsmb.1405

Eulalio, A., Tritschler, F. and Izaurralde, E. (2009). The GW182 protein family in animal cells: new insights into domains required for miRNA-mediated gene silencing. *RNA* **15**, 1433-1442. doi:10.1261/rna.1703809

Filipowicz, W., Bhattacharyya, S. N. and Sonenberg, N. (2008). Mechanisms of post-transcriptional regulation by microRNAs: are the answers in sight? *Nat. Rev. Genet.* **9**, 102-114. doi:10.1038/nrg2290

Ford, L., Ling, E., Kandel, E. R. and Fioriti, L. (2019). CPEB3 inhibits translation of mRNA targets by localizing them to P bodies. *Proc. Natl. Acad. Sci. USA* **116**, 18078-18087. doi:10.1073/pnas.1815275116

Gebert, L. F. R. and MacRae, I. J. (2019). Regulation of microRNA function in animals. *Nat. Rev. Mol. Cell Biol.* **20**, 21-37. doi:10.1038/s41580-018-0045-7

Georges, P. C., Hadzimichalis, N. M., Sweet, E. S. and Firestein, B. L. (2008). The Yin–Yang of dendrite morphology: unity of actin and microtubules. *Mol. Neurobiol.* **38**, 270-284. doi:10.1007/s12035-008-8046-8

Gorski, J. A., Zeiler, S. R., Tamowski, S. and Jones, K. R. (2003). Brain-derived neurotrophic factor is required for the maintenance of cortical dendrites. *J. Neurosci* **23**, 6856-6865. doi:10.1523/JNEUROSCI.23-17-06856.2003

Guerrini, R. and Mei, D. (2018). Unstable non-coding pentanucleotide repeats destabilize cortical excitability. *Brain* **141**, 2232-2235. doi:10.1093/brain/awy196

Hicks, J. A., Li, L., Matsui, M., Chu, Y., Volkov, O., Johnson, K. C. and Corey, D. R. (2017). Human GW182 paralogs are the central organizers for RNA-mediated control of transcription. *Cell Rep* **20**, 1543-1552. doi:10.1016/j.celrep.2017.07.058

Huang, Y.-W. A., Ruiz, C. R., Eyler, E. C. H., Lin, K. and Meffert, M. K. (2012). Dual regulation of miRNA biogenesis generates target specificity in neurotrophin-induced protein synthesis. *Cell* **148**, 933-946. doi:10.1016/j.cell.2012.01.036

Huang, Z.-M., Ge, H.-F., Yang, C.-C., Cai, Y., Chen, Z., Tian, W.-Z. and Tao, J.-L. (2019). MicroRNA-26a-5p inhibits breast cancer cell growth by suppressing RNF6 expression. *Kaohsiung J. Med. Sci.* **35**, 467-473.

Jakymiw, A., Lian, S., Eystathioy, T., Li, S., Satoh, M., Hamel, J. C., Fritzler, M. J. and Chan, E. K. L. (2005). Disruption of GW bodies impairs mammalian RNA interference. *Nat. Cell Biol.* **7**, 1267-1274. doi:10.1038/ncb1334

Jan, Y.-N. and Jan, L. Y. (2010). Branching out: mechanisms of dendritic arborization. *Nat. Rev. Neurosci.* **11**, 316-328. doi:10.1038/nrn2836

Jaworski, J., Spangler, S., Seeburg, D. P., Hoogenraad, C. C. and Sheng, M. (2005). Control of dendritic arborization by the phosphoinositide-3′-Kinase–Akt–mammalian target of rapamycin pathway. *J. Neurosci.* **25**, 11300-11312. doi:10.1523/JNEUROSCI.2270-05.2005

Kaech, S. and Banker, G. (2006). Culturing hippocampal neurons. *Nat. Protoc.* **1**, 2406-2415. doi:10.1038/nprot.2006.356

Keil, K. P., Miller, G. W., Chen, H., Sethi, S., Schmuck, M. R., Dhakal, K., Kim, J. W. and Lein, P. J. (2018). PCB 95 promotes dendritic growth in primary rat hippocampal neurons via mTOR-dependent mechanisms. *Arch. Toxicol.* **92**, 3163-3173. doi:10.1007/s00204-018-2285-x

Kenny, P. J., Zhou, H., Kim, M., Skariah, G., Khetani, R. S., Drnevich, J., Arcila, M. L., Kosik, K. S. and Ceman, S. (2014). MOV10 and FMRP regulate AGO2 association with microRNA recognition elements. *Cell Rep* **9**, 1729-1741. doi:10.1016/j.celrep.2014.10.054

Kosik, K. S. (2006). The neuronal microRNA system. *Nat. Rev. Neurosci.* **7**, 911-920. doi:10.1038/nrn2037

Kulkarni, V. A. and Firestein, B. L. (2012). The dendritic tree and brain disorders. *Mol. Cell. Neurosci.* **50**, 10-20. doi:10.1016/j.mcn.2012.03.005

Kumar, V., Zhang, M.-X., Swank, M. W., Kunz, J. and Wu, G.-Y. (2005). Regulation of dendritic morphogenesis by Ras–PI3K–Akt–mTOR and Ras–MAPK signaling pathways. *J. Neurosci* **25**, 11288-11299. doi:10.1523/JNEUROSCI.2284-05.2005

La Rocca, G., Olejniczak, S. H., González, A. J., Briskin, D., Vidigal, J. A., Spraggon, L., DeMatteo, R. G., Radler, M. R., Lindsten, T., Ventura, A., et al. (2015). In vivo, Argonaute-bound microRNAs exist predominantly in a reservoir of low molecular weight complexes not associated with mRNA. *Proc. Natl. Acad. Sci. USA* **112**, 767-772. doi:10.1073/pnas.1424217112

Lee, A., Li, W., Xu, K., Bogert, B. A., Su, K. and Gao, F.-B. (2003). Control of dendritic development by the Drosophila fragile X-related gene involves the small GTPase Rac1. *Development* **130**, 5543-5552. doi:10.1242/dev.00792

Lein, P. J. and Higgins, D. (1991). Protein synthesis is required for the initiation of dendritic growth in embryonic rat sympathetic neurons in vitro. *Dev. Brain Res.* **60**, 187-196. doi:10.1016/0165-3806(91)90047-M

Li, S., Wang, L., Fu, B., Berman, M. A., Diallo, A. and Dorf, M. E. (2014). TRIM65 regulates microRNA activity by ubiquitination of TNRC6. *Proc. Natl. Acad. Sci. USA* **111**, 6970-6975. doi:10.1073/pnas.1322545111

Lucci, C., Mesquita-Ribeiro, R., Rathbone, A. and Dajas-Bailador, F. (2020). Spatiotemporal regulation of GSK3β levels by miRNA-26a controls axon development in cortical neurons. *Development* **147**, dev180232. doi:10.1242/dev.180232

Martínez-Cerdeño, V. (2017). Dendrite and spine modifications in autism and related neurodevelopmental disorders in patients and animal models: dendrite and Spine in Autism. *Devel Neurobio* **77**, 393-404. doi:10.1002/dneu.22417

McAllister, A. K., Katz, L. C. and Lo, D. C. (1996). Neurotrophin regulation of cortical dendritic growth requires activity. *Neuron* **17**, 1057-1064. doi:10.1016/S0896-6273(00)80239-1

McNeill, E. and Van Vactor, D. (2012). microRNAs shape the neuronal landscape. *Neuron* **75**, 363-379. doi:10.1016/j.neuron.2012.07.005

Meijering, E., Jacob, M., Sarria, J.-C. F., Steiner, P., Hirling, H. and Unser, M. (2004). Design and validation of a tool for neurite tracing and analysis in fluorescence microscopy images. *Cytometry Part A* **58A**, 167-176. doi:10.1002/cyto.a.20022

Muddashetty, R. S., Nalavadi, V. C., Gross, C., Yao, X., Xing, L., Laur, O., Warren, S. T. and Bassell, G. J. (2011). Reversible inhibition of PSD-95 mRNA translation by miR-125a, FMRP phosphorylation and mGluR signaling. *Mol. Cell.* **42**, 673-688. doi:10.1016/j.molcel.2011.05.006

Nawalpuri, B., Ravindran, S. and Muddashetty, R. S. (2020). The role of dynamic miRISC during neuronal development. *Front. Mol. Biosci.* **7**, 8. doi:10.3389/fmolb.2020.00008

Niaz, S. and Hussain, M. U. (2018). Role of GW182 protein in the cell. *Int. J. Biochem. Cell Biol.* **101**, 29-38. doi:10.1016/j.biocel.2018.05.009

Olejniczak, S. H., Rocca, G. L., Radler, M. R., Egan, S. M., Xiang, Q., Garippa, R. and Thompson, C. B. (2016). Coordinated regulation of cap-dependent translation and MicroRNA function by convergent signaling pathways. *Mol. Cell. Biol.* **36**, 2360-2373. doi:10.1128/MCB.01011-15

Perycz, M., Urbanska, A. S., Krawczyk, P. S., Parobczak, K. and Jaworski, J. (2011). Zipcode binding protein 1 regulates the development of dendritic arbors in hippocampal neurons. *J. Neurosci* **31**, 5271-5285. doi:10.1523/JNEUROSCI.2387-10.2011

Pfaff, J., Hennig, J., Herzog, F., Aebersold, R., Sattler, M., Niessing, D. and Meister, G. (2013). Structural features of Argonaute–GW182 protein interactions. *PNAS* **110**, E3770-E3779. doi:10.1073/pnas.1308510110

Poulain, F. E. and Sobel, A. (2010). The microtubule network and neuronal morphogenesis: Dynamic and coordinated orchestration through multiple players. *Mol. Cell. Neurosci.* **43**, 15-32. doi:10.1016/j.mcn.2009.07.012

Rajgor, D., Sanderson, T. M., Amici, M., Collingridge, G. L. and Hanley, J. G. (2018). NMDAR–dependent Argonaute 2 phosphorylation regulates miRNA activity and dendritic spine plasticity. *EMBO J.* **37**, e97943. doi:10.15252/embj.201797943

Rajman, M. and Schratt, G. (2017). MicroRNAs in neural development: from master regulators to fine-tuners. *Development* **144**, 2310-2322. doi:10.1242/dev.144337

Ramakrishna, S. and Muddashetty, R. S. (2019). Emerging role of microRNAs in dementia. journal of molecular biology, dementia. *Brain Dis. Mol. Mech.* **431**, 1743-1762.

Ravindran, S., Nalavadi, V. C. and Muddashetty, R. S. (2019). BDNF induced translation of Limk1 in developing neurons regulates dendrite growth by fine-tuning cofilin1 activity. *Front. Mol. Neurosci* **12**, 64. doi:10.3389/fnmol.2019.00064

Saito, A., Miyajima, K., Akatsuka, J., Kondo, H., Mashiko, T., Kiuchi, T., Ohashi, K. and Mizuno, K. (2013). CaMKIIβ-mediated LIM-kinase activation plays a crucial role in BDNF-induced neuritogenesis. *Genes Cells* **18**, 533-543. doi:10.1111/gtc.12054

Schratt, G. M., Tuebing, F., Nigh, E. A., Kane, C. G., Sabatini, M. E., Kiebler, M. and Greenberg, M. E. (2006). A brain-specific microRNA regulates dendritic spine development. *Nature* **439**, 283-289. doi:10.1038/nature04367

Skalecka, A., Liszewska, E., Bilinski, R., Gkogkas, C., Khoutorsky, A., Malik, A. R., Sonenberg, N. and Jaworski, J. (2016). mTOR kinase is needed for the development and stabilization of dendritic arbors in newly born olfactory bulb neurons. *Dev. Neurobiol.* **76**, 1308-1327. doi:10.1002/dneu.22392

Slomnicki, L. P., Pietrzak, M., Vashishta, A., Jones, J., Lynch, N., Elliot, S., Poulos, E., Malicote, D., Morris, B. E., Hallgren, J., et al. (2016). Requirement of neuronal ribosome synthesis for growth and maintenance of the dendritic tree. *J. Biol. Chem.* **291**, 20. doi:10.1074/jbc.M115.682161

Sternburg, E. L., Estep, J. A., Nguyen, D. K., Li, Y. and Karginov, F. V. (2018). Antagonistic and cooperative AGO2-PUM interactions in regulating mRNAs. *Sci. Rep.* **8**, 15316. doi:10.1038/s41598-018-33596-4

Tursun, B., Schlüter, A., Peters, M. A., Viehweger, B., Ostendorff, H. P., Soosairajah, J., Drung, A., Bossenz, M., Johnsen, S. A., Schweizer, M., et al. (2005). The ubiquitin ligase Rnf6 regulates local LIM kinase 1 levels in axonal growth cones. *Genes Dev.* **19**, 2307-2319. doi:10.1101/gad.1340605

Wolterhoff, N., Gigengack, U. and Rumpf, S. (2020). PP2A phosphatase is required for dendrite pruning via actin regulation in Drosophila. *EMBO Rep.* **21**, e48870. doi:10.15252/embr.201948870

Xing, L., Yao, X., Williams, K. R. and Bassell, G. J. (2012). Negative regulation of RhoA translation and signaling by hnRNP-Q1 affects cellular morphogenesis. *Mol. Biol. Cell* **23**, 10. doi:10.1091/mbc.e11-10-0867

Xu, J., Du, Y.-L., Xu, J.-W., Hu, X., Gu, L., Li, X., Hu, P., Liao, T., Xia, Q., Sun, Q., et al. (2019). Neuroligin 3 regulates dendritic outgrowth by modulating Akt/mTOR signaling. *Front. Cell. Neurosci* **13**, 518. doi:10.3389/fncel.2019.00518

Yao, B., Li, S., Jung, H. M., Lian, S. L., Abadal, G. X., Han, F., Fritzler, M. J. and Chan, E. K. L. (2011). Divergent GW182 functional domains in the regulation of translational silencing. *Nucleic Acids Res.* **39**, 2534-2547. doi:10.1093/nar/gkq1099

Ye, B., Petritsch, C., Clark, I. E., Gavis, E. R., Jan, L. Y. and Jan, Y. N. (2004). . nanos and pumilio are essential for dendrite morphogenesis in Drosophila peripheral neurons. *Curr. Biol.* **14**, 314-321. doi:10.1016/j.cub.2004.01.052

Zielezinski, A. and Karlowski, W. M. (2015). Early origin and adaptive evolution of the GW182 protein family, the key component of RNA silencing in animals. *RNA Biol.* **12**, 761-770. doi:10.1080/15476286.2015.1051302

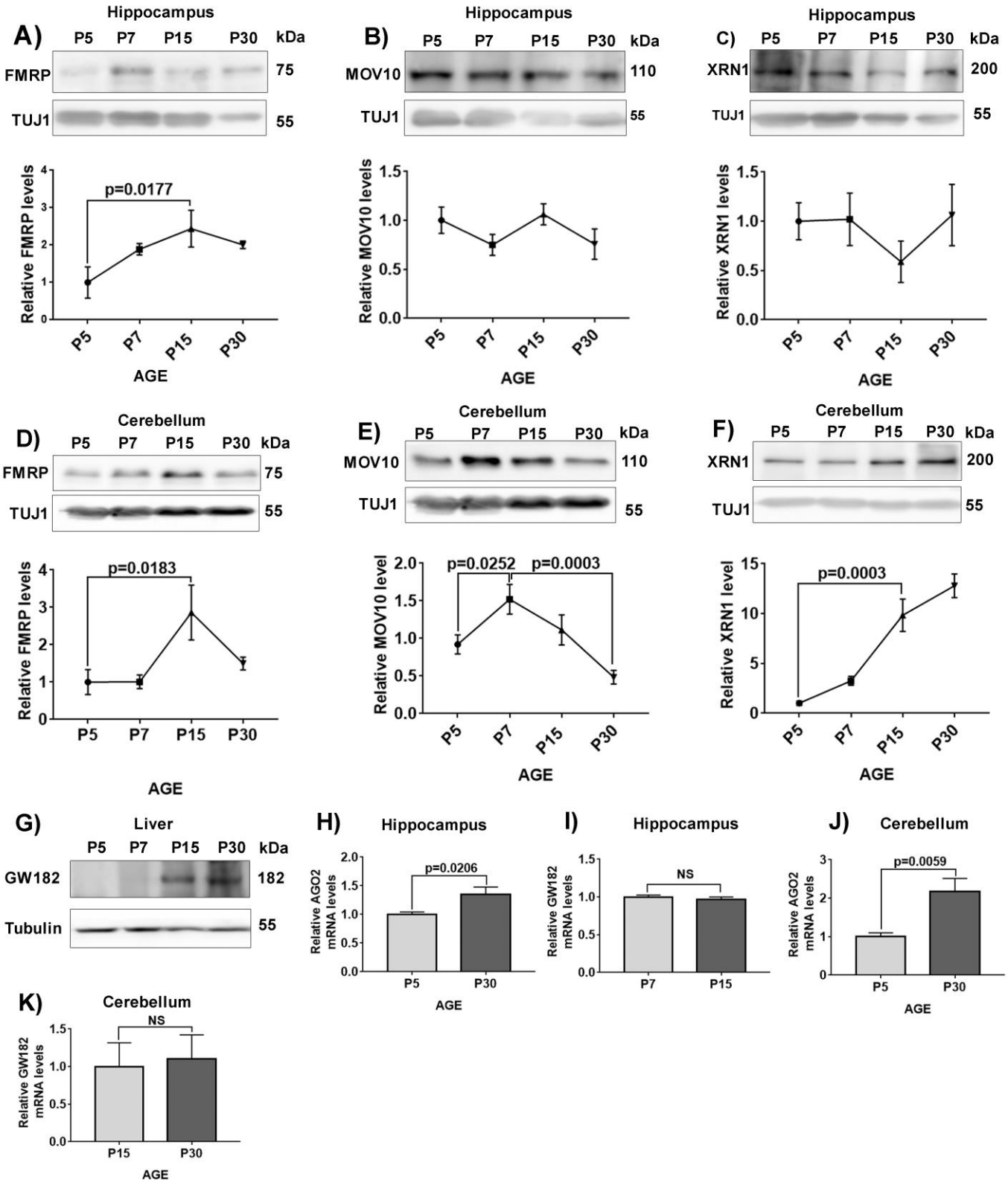

Fig. S1. A) Representative immunoblots (top) and line graph (bottom) depicting FMRP expression profile during hippocampal development. Data represent relative FMRP levels normalized to TUJ1, Data: mean +/- SEM, n=3-5 animals per group. One Way ANOVA followed by Bonferroni's multiple comparisons test.

B) Representative immunoblots (top) and line graph (bottom) depicting MOV10 expression profile during hippocampal development. Data represent relative MOV10 levels normalized to TUJ1, Data: mean +/- SEM, n=3-5 animals per group. One Way ANOVA followed by Bonferroni's multiple comparisons test.

C) Representative immunoblots (top) and line graph (bottom) depicting XRN1 expression profile during hippocampal development. Data represent relative XRN1 levels normalized to TUJ1, Data: mean +/- SEM, n=3-5 animals per group. One Way ANOVA followed by Bonferroni's multiple comparisons test.

D) Representative immunoblots (top) and line graph (bottom) depicting FMRP expression profile during Cerebellar development. Data represent relative FMRP levels normalized to TUJ1, Data: mean +/- SEM, n=3-5 animals per group. One Way ANOVA followed by Bonferroni's multiple comparisons test.

E) Representative immunoblots (top) and line graph (bottom) depicting MOV10 expression profile during Cerebellum development. Data represent relative MOV10 levels normalized to TUJ1, Data: mean +/- SEM, n=3-5 animals per group. One Way ANOVA followed by Bonferroni's multiple comparisons test.

F) Representative immunoblots (top) and line graph (bottom) depicting XRN1 expression profile during cerebellum development. Data represent relative XRN1 levels normalized to TUJ1, Data: mean +/- SEM, n=3-5 animals per group. One Way ANOVA followed by Bonferroni's multiple comparisons test.

G) Representative immunoblots depicting GW182 expression profile during liver development.

H) qPCR analysis of AGO2 mRNA expression in P5 and P30 hippocampus. The levels of AGO2 mRNA were normalized using the expression of ß-actin mRNA, Data: mean +/- SEM, n=3-5 independent experiments, Unpaired t-test.

I) qPCR analysis of GW182 mRNA expression in P7 and P15 hippocampus. The levels of GW182 mRNA were normalized using the expression of ß-actin mRNA, Data: mean +/- SEM, n=3-5 independent experiments, Unpaired t-test.

J) qPCR analysis of AGO2 mRNA expression in P5 versus P30 Cerebellum. The levels of AGO2 mRNA were normalized using the expression of ß-actin mRNA, Data: mean +/- SEM, n=3-5 independent experiments, Unpaired t-test.

K) qPCR analysis of GW182 mRNA expression in P15 versus P30 Cerebellum. The levels of GW182 mRNA were normalized using the expression of ß-actin mRNA, Data: mean +/- SEM, n=3-5 independent experiments, Unpaired t-test.

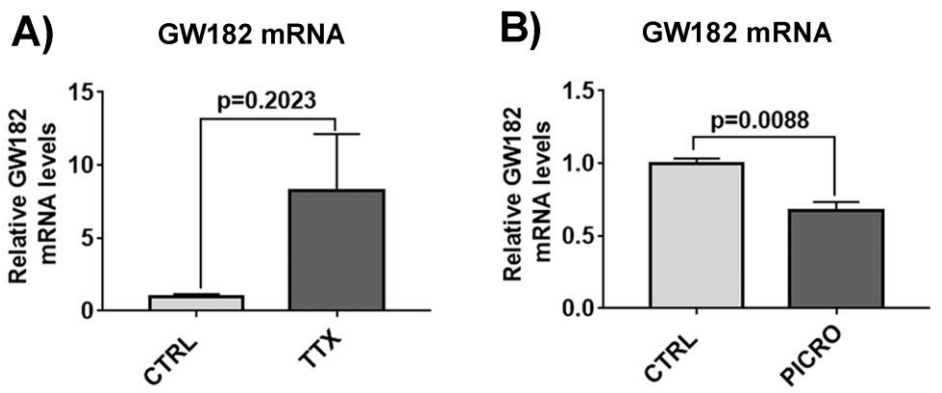

Fig. S2. A) qPCR analysis of GW182 mRNA expression from DIV7 hippocampal neurons treated with mock or tetradotoxin for 48hrs. The levels of GW182 mRNA were normalized using the expression of GAPDH mRNA, Data: mean +/- SEM, n=3 independent experiments, Unpaired t-test.

B) qPCR analysis of GW182 mRNA expression from DIV7 hippocampal neurons treated with mock or picrotoxin for 48hr. The levels of GW182 mRNA were normalized using the expression of GAPDH mRNA, Data: mean +/- SEM, n=3 independent experiments, Unpaired t-test

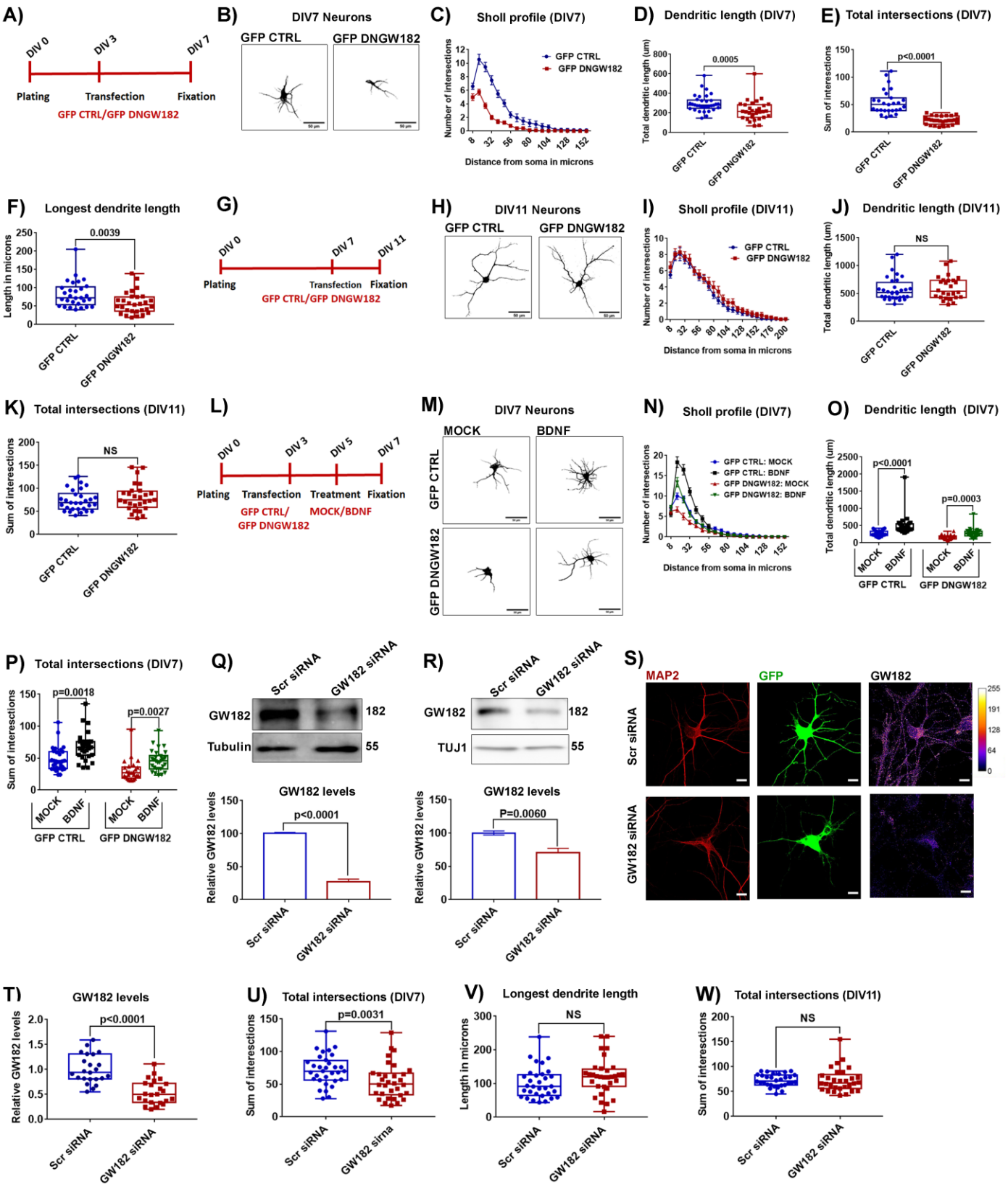

Fig. S3. A) Schematic showing the experimental procedure and timeline: Cultured hippocampal neurons were transfected with either control GFP or GFP DNGW182 on DIV3 and fixed on DIV7, followed by immunostaining.

B) Representative micrographs of DIV7 cultured hippocampal neurons transfected with either control GFP or GFP DNGW182 on DIV3. The images are derived from the threshold MAP2 intensity of transfected neurons. Scale bar represents 50 microns.

C) Sholl curve of DIV7 cultured hippocampal neurons transfected with either control GFP or GFP DNGW182 on DIV3. Data: mean +/- SEM, n=32 neurons from 4 independent experiments, GFP DNGW182 overexpressing neurons had significantly more dendrites from GFP overexpressing neurons at 16-48 microns from the soma, Two way ANOVA followed by Bonferroni's multiple comparisons test.

D) Quantification of the total dendritic length of cultured hippocampal neurons transfected with either control GFP vector or DN GW182 on DIV3, n=31-32 neurons from 4 independent cultures, Mann-Whitney test.

E) Quantification of total intersections of DIV7 hippocampal neurons transfected with either GFP or GFP DNGW182 on DIV 3, n=27 neurons from 3 independent cultures, Mann-Whitney test.

F) Quantification of the length of longest dendrite of DIV7 cultured hippocampal neurons transfected with either control GFP vector or DN GW182 on DIV3, n=29 neurons from 4 independent cultures, Mann-Whitney test.

G) Schematic showing the experimental procedure and timeline: Cultured hippocampal neurons were transfected with either control GFP or GFP DNGW182 on DIV7 and fixed on DIV11, followed by immunostaining.

H) Representative micrographs of DIV11 cultured hippocampal neurons transfected with either control GFP vector or GFP DNGW182 mutant on DIV7. The images are derived from the threshold MAP2 intensity of transfected neurons. Scale bar represents 50 microns.

I) Sholl curve of DIV11 cultured hippocampal neurons transfected with either control GFP or GFP DNGW182 mutant on DIV7. Data: mean +/- SEM, n=22-25 neurons from 4 independent experiments.

J) Quantification of the total dendritic length of DIV11 cultured hippocampal neurons transfected with either Control GFP or GFP DNGW182 on DIV7, n=26-32 neurons from 4 independent cultures, Mann-Whitney test.

K) Quantification of total intersections of DIV11 hippocampal neurons transfected with either GFP or GFP DNGW182 on DIV7, n=28-30 neurons from 4 independent cultures, Unpaired t-test with Welch's correction.

L) Schematic showing the experimental procedure and timeline: Cultured hippocampal neurons were transfected on DIV3 followed by BDNF treatment for 48hrs starting from DIV5 onwards, and fixed on DIV7.

M) Representative images of cultured hippocampal neurons transfected at DIV3 with either control GFP or GFP DNGW182. After transfection, the neurons were treated with BDNF (50ng/ml) on DIV 5 and were fixed on DIV7. Scale bar represents 50 microns.

N) Sholl Quantification of the effects of GFP DNGW182 on BDNF-induced dendrite arborization formation of hippocampal neurons. Data: mean +/- SEM, n=25-30 neurons from 4 independent experiments, BDNF treatment resulted in increased dendritic intersections in GFP transfected neurons at 16-40 microns from the soma and resulted in increased intersections in GFP DNGW182 transfected neurons as well at 16-32 microns from the soma, Two way ANOVA followed by Bonferroni's multiple comparisons test.

O) Quantification of the total dendritic length of neurons described in Figure S3R, n=25-30 neurons from 3 independent experiments, Kruskal- Wallis followed by Dunn's multiple comparisons test.

P) Quantification of total intersections of MOCK/BDNF treated (48 hrs) DIV7 hippocampal neurons transfected with either GFP or GFP DNGW182, n=25-30 neurons from 3 independent cultures, Kruskal- Wallis followed by Dunn's multiple comparisons test.

Q) Immunoblot validation of GW182 knockdown in Neuro2A cells: Representative immunoblots (top) and quantification (bottom) of GW182 levels from N2A cells treated with either scrambled or GW182 siRNA. Data: mean +/- SEM, n=3 independent experiments, Unpaired t-test.

R) Immunoblot validation of GW182 knockdown in cultured hippocampal neurons: Representative immunoblots (top) and quantification (bottom) of GW182 levels from cultured hippocampal neurons cells treated with either scrambled or GW182 siRNA. Data: mean +/- SEM, n=4 independent cultures, Unpaired t-test.

S) Immunostaining validation of GW182 knockdown in hippocampal neuronal culture: Representative images showing GW182 staining in DIV5 hippocampal cultured neurons transfected with GFP along with either scrambled siRNA or GW182 siRNA on DIV3.

T) Immunostaining quantification representing GW182 levels in neurons upon scrambled siRNA or GW182 siRNA transfections. Data: mean +/- SEM, n=23-24 neurons from 3 independent cultures, Unpaired t-test.

U) Quantification of total intersections of DIV7 hippocampal neurons transfected with either scrambled siRNA or GW182 siRNA on DIV3, n=32 neurons from 4 independent cultures, Unpaired t-test.

V) Quantification of length of longest dendrite of DIV7 hippocampal neurons transfected with either scrambled siRNA or GW182 siRNA on DIV3, n=32 neurons from 4 independent cultures, Unpaired t-test.

W) Quantification of total intersections of DIV11 hippocampal neurons transfected with either scrambled siRNA or GW182 siRNA on DIV7, n>25 neurons from 4 independent cultures, Unpaired t-test with Welch's correction.

Journal of Cell Science • Supplementary information

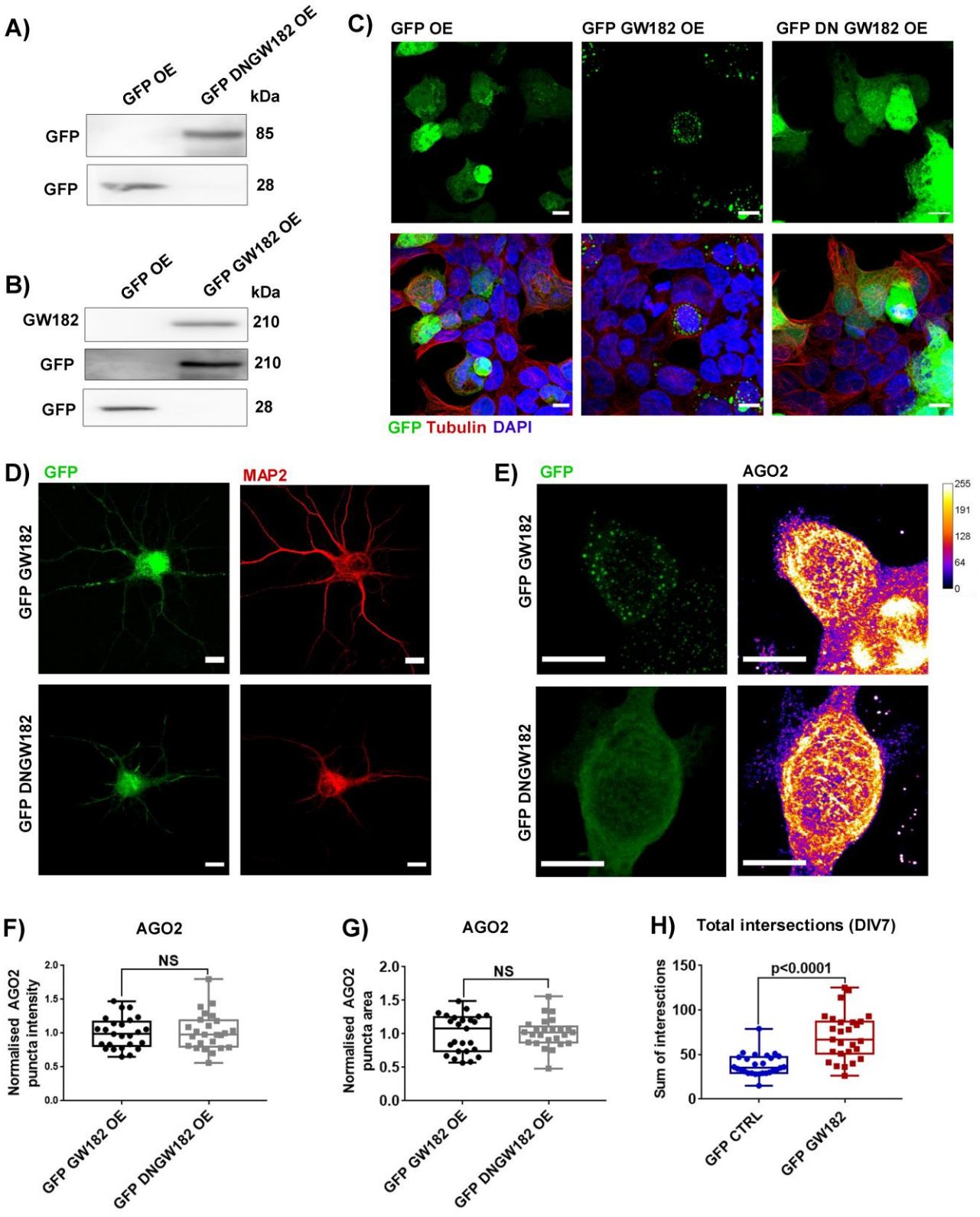
A)
GFP OE
GFP DNGW182 OE
kDa
GFP
85
GFP
28
B)
GFP OE
GFP GW182 OE
kDa
GW182
210
GFP
210
GFP
28
C)
GFP OE
GFP GW182 OE
GFP DN GW182 OE
GFP Tubulin DAPI
D)
GFP
MAP2
GFP GW182
GFP DNGW182
E)
GFP
AGO2
GFP GW182
GFP DNGW182
255
191
128
64
0
F)
AGO2
NS
Normalised AGO2 puncta intensity
2.0
1.5
1.0
0.5
0.0
GFP GW182 OE
GFP DNGW182 OE
G)
AGO2
NS
Normalised AGO2 puncta area
2.0
1.5
1.0
0.5
0.0
GFP GW182 OE
GFP DNGW182 OE
H)
Total intersections (DIV7)
p<0.0001
Sum of intersections
150
100
50
0
GFP CTRL
GFP GW182

Fig. S4.

A) Immunoblot validation of GFP DNGW182 overexpression in HEK293T cells using GFP antibody.

B) Immunoblot validation of GFP GW182 overexpression in HEK293T cells using GFP and GW182 antibody.

C) Immunostaining characterization of GFP GW182 and GFP DNGW182 overexpression in HEK293T cells. Cells were stained with DAPI and tubulin to identify nuclear and cytosolic compartments. Scale bar represents 10 microns.

D) Immunostaining Validation of GFP GW182 and GFP DNGW182 overexpression in cultured hippocampal neurons. Neurons were identified using MAP2 staining. Scale bar represents 10 microns.

E) Representative images showing AGO2 staining in GFP GW182 or GFP DN GW182 transfected HEK293T cells.

F) Quantification of AGO2 puncta intensity in GFP GW182 or GFP DN GW182 transfected HEK293T cells, n=23 cells from two independent experiments.

G) Quantification of AGO2 puncta area in GFP GW182 or GFP DN GW182 transfected HEK293T cells, n=23 cells from two independent experiments

H) Quantification of total intersections of DIV7 hippocampal neurons transfected with either GFP or GFP GW182 at DIV 3, n=27 neurons from 3 independent cultures, Mann-Whitney test.

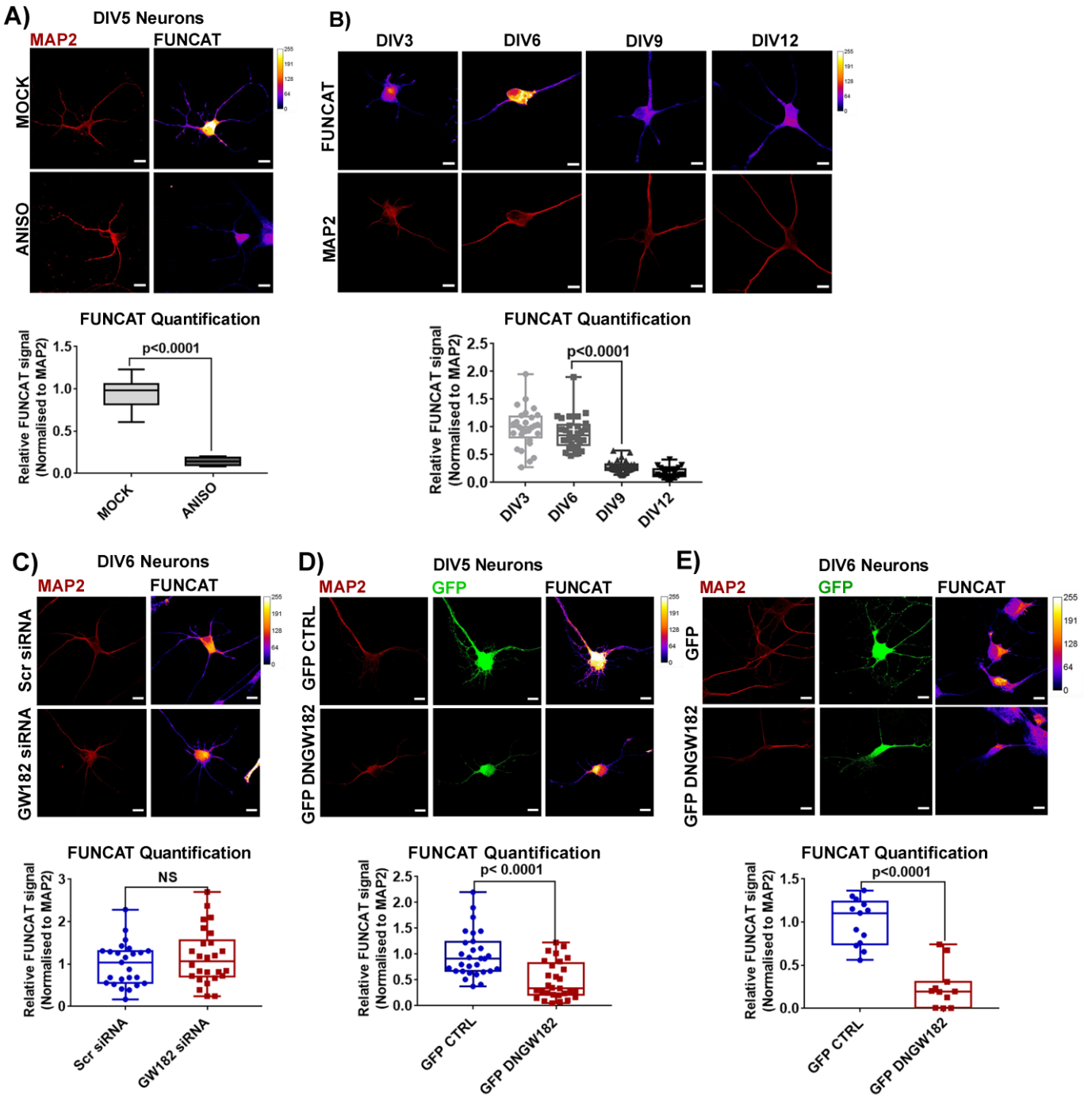
A)
DIV5 Neurons
MAP2
FUNCAT
MOCK
ANISO
FUNCAT Quantification
Relative FUNCAT signal (Normalised to MAP2)
p<0.0001
MOCK
ANISO
B)
DIV3
DIV6
DIV9
DIV12
FUNCAT
MAP2
FUNCAT Quantification
Relative FUNCAT signal (Normalised to MAP2)
p<0.0001
DIV3
DIV6
DIV9
DIV12
C)
DIV6 Neurons
MAP2
FUNCAT
Scr siRNA
GW182 siRNA
FUNCAT Quantification
Relative FUNCAT signal (Normalised to MAP2)
NS
Scr siRNA
GW182 siRNA
D)
DIV5 Neurons
MAP2
GFP
FUNCAT
GFP CTRL
GFP DNGW182
FUNCAT Quantification
Relative FUNCAT signal (Normalised to MAP2)
p< 0.0001
GFP CTRL
GFP DNGW182
E)
DIV6 Neurons
MAP2
GFP
FUNCAT
GFP
GFP DNGW182
FUNCAT Quantification
Relative FUNCAT signal (Normalised to MAP2)
p<0.0001
GFP CTRL
GFP DNGW182

Fig. S5. A) Representative FUNCAT images (top) and corresponding quantification (bottom) of either Mock or Anisomycin treated DIV5 cultured hippocampal neurons, Scale bar represents 10 microns, n=6 neurons from 1 experiment, Unpaired t-test.

B) Representative FUNCAT images (top) and corresponding quantification (bottom) showing FUNCAT signal across different stages of hippocampal neuron development. Scale bar represents 10 microns, n=29-32 neurons from 3 independent cultures, Kruskal-allis test along with Dunn's multiple comparison test.

C) Representative FUNCAT images (top) and corresponding quantification (bottom) of FUNCAT signal (Normalized to corresponding MAP2 signal) in DIV6 cultured hippocampal neurons, transfected with either Scrambled siRNA or GW182 siRNA on DIV3, Scale bar represents 10 microns, n=26 neurons from 3 independent experiments, Unpaired t-test.

D) Representative FUNCAT images (top) and corresponding quantification (bottom) of FUNCAT signal (Normalized to corresponding MAP2 signal) in DIV5 cultured hippocampal neurons, transfected with either GFP control or GFP DNGW182 on DIV3, Scale bar represents 10 microns, n=29 neurons from 3 independent experiments, Mann-Whitney test.

E) Representative FUNCAT images (top) and corresponding quantification (bottom) of FUNCAT signal (Normalized to corresponding MAP2 signal) in DIV6 cultured hippocampal neurons, transfected with either GFP control or GFP DNGW182 on DIV3, Scale bar represents 10 microns, n=25-30 neurons from 3 independent experiments, Unpaired t-test.

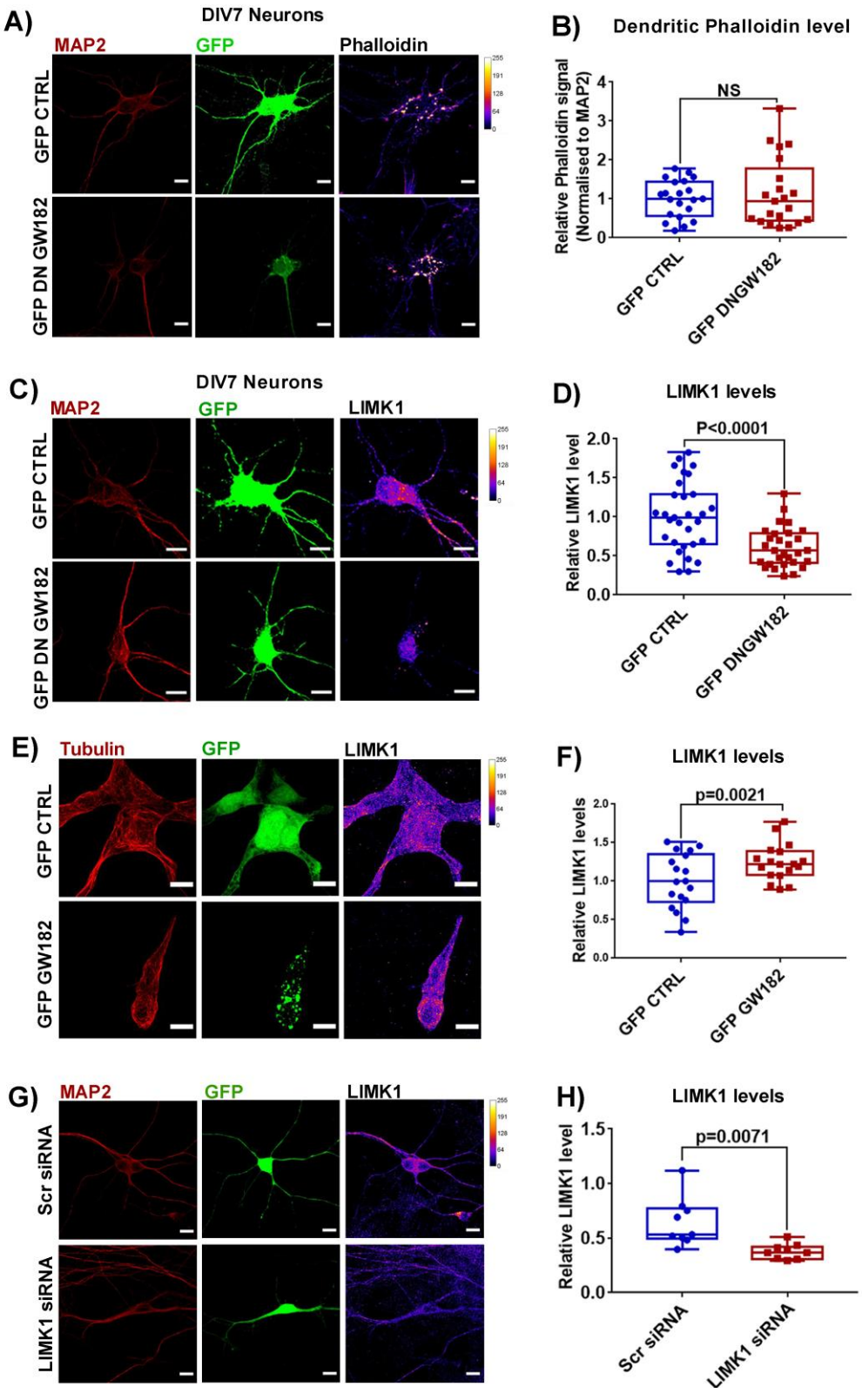
A)
DIV7 Neurons
MAP2
GFP
Phalloidin
GFP CTRL
GFP DN GW182
B)
Dendritic Phalloidin level
Relative Phalloidin signal (Normalised to MAP2)
NS
GFP CTRL
GFP DNGW182
C)
DIV7 Neurons
MAP2
GFP
LIMK1
GFP CTRL
GFP DN GW182
D)
LIMK1 levels
P<0.0001
Relative LIMK1 level
GFP CTRL
GFP DNGW182
E)
Tubulin
GFP
LIMK1
GFP CTRL
GFP GW182
F)
LIMK1 levels
p=0.0021
Relative LIMK1 levels
GFP CTRL
GFP GW182
G)
MAP2
GFP
LIMK1
Scr siRNA
LIMK1 siRNA
H)
LIMK1 levels
p=0.0071
Relative LIMK1 level
Scr siRNA
LIMK1 siRNA
I)
Total intersections
NS
p<0.0001
p=0.0262
Sum of intersections
Scr siRNA
LIMK1 siRNA
Scr siRNA
LIMK1 siRNA
GFP CTRL
GFP GW182

Fig. S6. A) Representative images of DIV7 cultured hippocampal neurons showing Phalloidin staining in GFP control or GFP DNGW182 transfected neurons. Scale bar represents 10 microns.

B) Quantification of Phalloidin intensity (Normalized to corresponding MAP2 signal) in GFP control or GFP DNGW182 transfected neurons, n=21 neurons from 3 independent experiments, Unpaired t-test with Welch's correction.

C) Representative images of DIV7 cultured hippocampal neurons showing LIMK1 staining in GFP control or GFP DNGW182 transfected neurons. Scale bar represents 10 microns.

D) Quantification of normalized LIMK1 signal in GFP control or GFP DNGW182 transfected neurons. n=29-31 neurons from 4 independent experiments, Unpaired t-test with Welch's correction.

E) Representative images showing LIMK1 staining in HEK293T cells with either GFP or GFP GW182 overexpression. Scale bar represents 10 microns.

F) Quantification of LIMK1 intensity in GFP or GFP GW182 overexpressing HEK293T cells. n=18 cells, from 2 independent experiment, unpaired t-test.

G) Immunostaining validation of LIMK1 siRNA in cultured hippocampal neurons using LIMK1 antibody. Scale bar represents 10 microns.

H) Quantification of LIMK1 intensity (Normalized to MAP2 intensity of corresponding neurons) in neurons transfected with either scrambled siRNA or LIMK1 siRNA. n=9 neurons from 1 experiment, unpaired t-test with Welch's correction.

I) Quantification of total intersections of cultured hippocampal neurons transfected with either control GFP or GFP GW182 along with scrambled or LIMK1 siRNA. n=26-27 neurons from 3 independent experiments, Kruskal-Wallis followed by Dunn's multiple comparisons test.

Table S1. List of primers used in the study.

List of primers		
Transcript	**Forward primer (5'-3')**	**Reverse primer (5'-3')**
GAPDH	CAACTCCCTCAAGATTGTCAGCA	GGCATGGACTGTGGTCATGA
β-ACTIN	GGCTCCTAGCACCATGAAGAT	AAACGCAGCTCAGTAACAGTC
TNRC6A	ACACCTCAGATTGACGGCTC	AGCATTTCCATGTGGGAGGTT
AGO2	TGAGCGGGTTGGAAAGAGTG	TAAGCTGGCGCAGGAATTGA